Westinghouse

WNSD/HYDRO-89-06

METAL TRANSFER IN GAS METAL ARC WELDING

Donald M. McEligot
Hydrothermodynamics Research and Technology
Westinghouse Electric Corportion
Naval Systems Division
(formerly Gould/Ocean Systems Division)
62 Johnnycake Hill
Middletown, Rhode Island 02840

30 September 1989

Final Report for Period 21 September 1988 to 30 September 1989
Contract Number N00014-88-C-0393

Prepared for
MATERIALS SCIENCE PROGRAM
OFFICE OF NAVAL RESEARCH (Code 1131M)
800 North Quincy Street
Arlington, Virginia 22217-5000

UNCLASSIFIED

SECURITY CLASSIFICATION OF THIS PAGE

REPORT DOCUMENTATION PAGE

1a REPORT SECURITY CLASSIFICATION Unclassified	1b RESTRICTIVE MARKINGS
2a SECURITY CLASSIFICATION AUTHORITY	3 DISTRIBUTION / AVAILABILITY OF REPORT APPROVED FOR PUBLIC RELEASE: DISTRIBUTION IS UNLIMITED.
2b DECLASSIFICATION / DOWNGRADING SCHEDULE	
4 PERFORMING ORGANIZATION REPORT NUMBER(S) WNSD/HYDRO-89-06	5 MONITORING ORGANIZATION REPORT NUMBER(S)
6a NAME OF PERFORMING ORGANIZATION Westinghouse Electric Corp. Naval Systems Division 6b OFFICE SYMBOL (If applicable)	7a NAME OF MONITORING ORGANIZATION DCASPRO-Westinghouse
6c ADDRESS (City, State, and ZIP Code) Hydrothermodynamics Research and Technology 62 Johnnycake Hill Middletown, RI 02840	7b ADDRESS (City, State, and ZIP Code) c/o Westinghouse Oceanic Division 18901 Euclid Avenue Cleveland Ohio 44117 0668
8a NAME OF FUNDING / SPONSORING ORGANIZATION Office of Naval Research 8b OFFICE SYMBOL (If applicable) Code 1131M	9 PROCUREMENT INSTRUMENT IDENTIFICATION NUMBER N00014-88-C-0393
8c ADDRESS (City, State, and ZIP Code) 800 N. Quincy Street Arlington, VA 22217	10 SOURCE OF FUNDING NUMBERS PROGRAM ELEMENT NO / PROJECT NO / TASK / WORK UNIT ACCESSION NO

11 TITLE (Include Security Classification)

Metal Transfer in Gas Metal Arc Welding

12 PERSONAL AUTHOR(S)

Donald M. McEligot

13a TYPE OF REPORT	13b TIME COVERED	14 DATE OF REPORT (Year, Month, Day)	15 PAGE COUNT
Final Report	FROM 21 Sep88 TO 30 Sep89	89 Sep 30	124

16 SUPPLEMENTARY NOTATION

17 COSATI CODES			18 SUBJECT TERMS (Continue on reverse if necessary and identify by block number)
FIELD	GROUP	SUB-GROUP	Welding; GMAW; Heat transfer; Metal transfer; Droplet; Detachment; Melting; Numerical predictions; (Gas Metal Arc Welding; GMA)

19 ABSTRACT (Continue on reverse if necessary and identify by block number)

The ultimate goal of the present work is to develop sufficient fundamental understanding of generic GMA welding to enable prediction of the weld quality to be made in terms of the material properties and control parameters. Evidence from experiments and simple analyses shows that the melting rate is controlled by the thermofluidmechanic behavior of the solid electrode and the molten electrode tip. Consequently, an analytical and numerical study of the transient, thermalfluidmechanic behavior of the electrode region in GMA welding continues. The present report discusses two idealized regions separately: (1) steady thermal conduction in a moving solid electrode and (2) transient droplet formation. The method of superposition and classical techniques were used to describe the temperature distribution in an electrode heated on the side by electron condensation. A transient numerical analysis for the liquid droplet or streaming jet is being developed using LaGrangian governing equations. ...

20 DISTRIBUTION / AVAILABILITY OF ABSTRACT	21 ABSTRACT SECURITY CLASSIFICATION
☒ UNCLASSIFIED/UNLIMITED ☒ SAME AS RPT ☐ DTIC USERS	
22a NAME OF RESPONSIBLE INDIVIDUAL Dr. George R. Yoder	22b TELEPHONE (Include Area Code) (202) 696-0282 22c OFFICE SYMBOL ONR Code 1131M

DD FORM 1473, 84 MAR 83 APR edition may be used until exhausted
All other editions are obsolete

SECURITY CLASSIFICATION OF THIS PAGE
UNCLASSIFIED

METAL TRANSFER IN GAS METAL ARC WELDING

Abstract

Gas metal arc welding has become the most common method for arc welding steels, superalloys, aluminum and reactive metals, yet the behavior of the interacting physical phenomena which determine the weld quality are not yet understood well. About forty percent of the production welding in this country is accomplished by this process; in naval ship construction worldwide the percentage is higher and more will be necessary for HY-100 and HY-130.

The ultimate goal of the present work is to develop sufficient fundamental understanding of generic GMA welding to enable prediction of the weld quality to be made in terms of the material properties and control parameters. Evidence from experiments and simple analyses shows that the melting rate is controlled by the thermofluidmechanic behavior of the solid electrode and the molten electrode tip. Consequently, an analytical and numerical study of the transient, thermalfluidmechanic behavior of the detachment phase for metal transfer in GMA welding has been initiated. Current studies concentrate on two idealized regions to ease physical insight into the overall problem: (1) steady thermal conduction in the moving electrode and (2) transient droplet formation. Emphasis is on applications for steel electrodes.

The previous report, for the first half year of the study, reviewed the related background and then concentrated on approximate and time scales analyses preparatory to the development of a transient, axisymmetric numerical analysis to describe droplet detachment in globular and spray modes. These analyses did not reveal any significant simplifications which would be appropriate for the governing partial differential equations. Highlights are included in Appendix A of the present report.

To account for heating of the side surfaces by electron condensation in argon shielding of steel electrodes, a closed form analysis of thermal conduction in moving electrodes was derived. The method of superposition was applied with a basic solution for uniform internal energy generation (resistive heating) with a step change in surface heat flux (electron condensation). The resulting superposition integral allows treating any reasonable axial surface heating distribution chosen to represent the phenomenon.

Scales to non-dimensionalize the droplet variables were defined in terms of the liquid steel properties; they are approximately 1/2 inch, 400 in/min and 30 ms. If the non-dimensional product $r_w V_{in}^2$ is much less than one, droplets are expected to form; if greater, then steady jets should occur. This corresponds to globular-spray and streaming transfer, respectively. A one-dimensional, transient numerical analysis, using a LaGrangian representation, is being developed to describe this range of metal transfer modes.

TABLE OF CONTENTS

NOMENCLATURE

A_{cs}	Cross-sectional area
A_s	Surface area
c_p	Specific heat at constant pressure
D,d	Diameter
e	Electron charge
g	Acceleration of gravity
g_c	Unit conversion factor
H	Specific enthalpy
h	Convective heat transfer coefficient, $q_s''/(T_w - T_f)$
I	Specific internal thermal energy
i	Electrical current
J	Electrical current density, i/A_{cs}
k	Thermal conductivity
L	Characteristic length; also length of electrode from contact tip to arc-molten metal interface
$\dot{m}$	Mass flow rate; melting rate
P	Period
q	Energy rate (power) or heat transfer rate; q_G, total resistive heating; q_{EC}, energy absorbed on side surfaces due to electron condensation; q_{L-S}, required from liquid drop to liquid-solid interface
q	Electron charge
q_G'''	Volumetric energy generation rate (resistive heating per unit volume)
q_s''	Surface heat flux
r	Radial distance; r_o, outside radius
T	Absolute temperature; T_r, reference or room temperature; T_o, amplitude of temperature fluctuations

t	Time; relative temperature (e.g.,°C)
u	Velocity component in axial direction
V	Voltage; V_c, apparent condensation voltage; V_a, anode voltage drop
V	Uniform or bulk velocity; V_w, electrode (wire) feed velocity
v	Velocity component in radial direction
x	Axial distance
z	Axial distance, measured from molten tip, L-x

Non-dimensional parameters

Bd, Bo, Bo_d	Bond numbers for thermocapillary phenomena [Lai, Ostrach and Kamotani, 1985], see text Sec. 2. - Appendix A
Bi	Biot number, $h \cdot Vol/(A_s \cdot k_{solid})$
Pe	Peclet number, $Pr \cdot Re = Vd/\alpha$
Pr	Prandtl number, $c_p\mu/k$
Re	Reynolds number, $4\dot{m}/(\pi D\mu)$

Greek letters

α	Fraction of total electron condensation absorbed on electrode side surface; thermal diffusivity, $k/\rho c_p$
β	Volumetric coefficient of thermal expansion
θ	Time scale; θ_T, thermal; θ_V, viscous
μ	Viscosity
ν	Kinematic viscosity, μ/ρ
ρ	Density; ρ_l, liquid density
ρ_e	Electrical resistivity

NOMENCLATURE - Continued

Greek letters - continued

σ	Surface tension; Gaussian distribution parameter
ϕ	Work function of material (volts)

Subscripts

j	Liquid-solid interface
in	Evaluated at inlet to region considered, e.g., at $x = 0$
s	Evaluated at surface conditions
w	Wire (electrode)

Note: Some additional symbols used only locally in text are defined where they are used.

METAL TRANSFER IN GAS METAL ARC WELDING

1. INTRODUCTION

Gas Metal Arc (GMA) welding is the major method for welding steels, super-alloys and aluminum; about forty percent of the production welding in this country is accomplished by this process. In this process the thermal phenomena and melting of the solid electrode are coupled to the plasma arc and weld pool. Thus, the thermalfluid behavior of the electrode and detaching drops can have significant effects on the consequent weld quality and production rate.

In naval ship construction a greater percentage of the welding is by GMA, and more will be necessary for HY-100 and HY-130. Yet the behavior of the interacting physical phenomena, which determine the weld quality in this complicated process, are not yet understood well.

GMA welding is important in the construction of Naval ships and submersibles. For example, the operating depth of submersibles can be increased by a factor of two by using titanium alloys [Masubuchi and Terai, 1976] if reliable welds can be insured. The gas tungsten arc (GTA) process has proved to be reliable but slow. In order to be used in a production shipyard environment, automatic and manual all-position GMA processes need to be developed.

While a number of qualitative hypotheses concerning metal transfer have been suggested and in some instances accepted, quantitative proof of their

validity is still lacking [Eagar, 1989]. A purpose of the present study is to provide quantitative analyses, concentrating on the thermal behavior of the solid electrode and molten drop to aid fundamental understanding of the process.

1.1 Related studies

For a general review of recent work on metal transfer, the reader is referred to Lancaster's chapter in the text by Study Group 212 of the International Institute of Welding [Lancaster, 1984]. A brief literature review is also included in our last report [McEligot and Uhlman, 1988]. The classical pioneering study of metal transfer by Lesnewich [1958a, b] has been recently summarized by him in a letter [Lesnewich, 1987]. Cooksey and Miller [1962] described six modes and Needham and Carter [1965] defined the ranges of metal transfer. Weld quality depends on the mode occurring. The axial spray transfer mode is preferred for gas-shielded metal-arc welding to insure maximum arc stability and minimum spatter.

Analyses and experiments have been conducted by Greene [1960], Halmoy [1980], Woods [1980], Ueguri, Hara and Komura [1985], Allum [1985] and by Waszink and coworkers [1982, 1983, 1985, 1986]. These studies have predominantly addressed steady or static conditions, although Lancaster and Allum did consider transient instabilities for possible explanations of the final stage of the droplet detachment process.

Tests by AirCo approximately three decades ago showed that various additives on the surface of welding rods could cause significant variations in the deposition rate [Cameron and Raeslack, 1956]. One likely effect of such additives would be a modification of the surface tension of the liquid metal in

the droplet. In comparable experiments with GTA weld pools, Heiple and Roper [1982] demonstrated that such alteration of surface tension gradients changed the fluid flow patterns and the fusion zone geometry significantly. Thus, it is anticipated that surface-tension-driven flow ("Marangoni convection") [Levich and Krylov, 1969; Ostrach, 1977, 1983] induced by temperature gradients in the molten droplet will also have a significant effect on the droplet formation, flow and detachment and, therefore, on the metal transfer rate.

DTRC and INEL [Johnson, Carlson and Smartt, 1989] are conducting visualization experiments plus studies of signals from electric, audio and acoustic sensors. Droplet detachment events observed on film or video can be correlated with the sensor data. Audio, current and voltage data can be used to discriminate between modes of transfer: globular, spray and streaming. Detachment frequencies can be observed for globular and spray modes, but little information is observed in the digitized data for streaming transfer. Usually, no abrupt transition [Lesnewich, 1958] is observed [Morris, 1989; Kim, 1989]. In recent studies Chen and colleagues [1989] have studied the mechanism of globular metal transfer from covered electrodes. Liu and Siewert [1989] examined metal transfer in the short circuiting mode.

Recently Kim [1989 and Appendix A of present report (part)] explored the effects of welding parameters on metal transfer phenomena in GMAW. Droplet sizes were measured by high speed videography and were compared with sizes predicted by a static force balance theory and the pinch instability theory. The comparison showed that the droplet size predicted from the static force balance theory can predict the droplet size reasonably well in the range of globular transfer, but deviated significantly in the range of spray transfer. The cause of the deviation was found to be due to tapering of the electrode tip

during welding. Heat transfer mechanisms in the solid electrode were studied in order to couple metal transfer with conduction heat transfer. Electrode melting rates were measured. It was found that a previously proposed theory was inadequate to explain electrode melting behavior. Using a more complete temperature distribution model of the electrode, a new model of electrode melting was proposed that agrees with the experimentally measured melting rates. Combining the results of droplet size prediction and the electrode melting rate measurements, a new treatment of pulsed current GMAW was proposed. A theoretical pulsing frequency may be predicted by this new theory. For given pulse parameters, experimental results show that there is a range of optimum pulsing frequency and that this optimum pulsing frequency can be predicted using the theoretical pulsing frequency and natural drop transfer frequency. The pulsing parameters were also varied to investigate the effect of tapering of the electrode on the droplet size in pulsed current welding and experimental results were used to support the theory for modeling the droplet size in pulsed current GMAW.

A number of computational fluid mechanics studies have been applied to "simple" liquid drop formation other than in GMAW. Daly [1969] developed numerical marker-and-cell techniques for handling free surfaces and demonstrated their capabilities by application to the Rayleigh-Taylor instability of a heavy fluid above a light fluid as occurs in GMAW. Fromm [1984] applied a comparable transient, axisymmetric numerical technique to predict liquid jet formation from nozzles and breakup into individual droplets for "drop-on-demand" ink jet printers. Adams and Roy [1986] developed a one-dimensional unsteady treatment of the same phenomena as Fromm and verified it by comparison to Fromm's predictions. Adams [1989] reports that their code is now used routinely for design calculations and is reasonably rapid. While their studies lack consideration

of heat transfer, gravity and electromagnetic forces, they do include some aspects which are important in the GMAW problem of droplet detachment.

Sunmewa and Mucolu [1985] in Japan have shown that the electrode wire melting rate can also be increased by increasing the ambient pressure at which the GMA operation is conducted. The basic phenomena accounting for this increase have not been identified.

From experiments and simple analyses at Philips Research Laboratories, Waszink and Piena [1985] concluded that, for covered electrodes, the melting rate is controlled by electromagnetically-induced fluid flow in the electrode tip. However, they estimated that for the conditions of their experiments surface tension forces and buoyancy forces were of the same order-of-magnitude as electromagnetic forces, i.e., 1:1:3. Therefore, since they consider convection in the droplet to be important in the detachment process, we have proposed to conduct an analytical and numerical study of the transient thermalfluidmechanic behavior of this process in GMA and to examine the validity of the results by comparison to measurements at DTEC and MIT. Both "steady" and pulsed operation would be studied.

1.2 Goal and Objective

Our general goal is to develop sufficient fundamental understanding of generic GMA welding to enable prediction of the weld quality to be made in terms of the material properties and control parameters for metals and alloys important in practical situations. Accomplishment of this goal ultimately requires understanding of the weld pool, plasma and droplet regions and their interactions.

The immediate objective of the proposed work is to develop the necessary basic knowledge of the thermalfluidmechanical behavior of the solid moving electrode and its droplet region (or electrode tip).

Potential consequences of this knowledge are controllable increases in melting or welding rate, understanding of the mechanism of transition from subthreshold to "normal mode" of droplet detachment, reduction of spatter, quantitative evaluation of present qualitative hypotheses, reduction of smoke or fume formation, etc. In addition, if the mechanism of enhanced electrode melting rate experienced by Cameron and Baeslack (and others since then) could be understood and controlled, it would permit up to 20 or 30 percent increases in GMA weld productivity. If this is accomplished at essentially the same welding heat input, it would permit welding of higher strength materials which are ordinarily degraded by current arc welding processes. Such gains in productivity and weldability of advanced materials would have tremendous economic impact.

1.3 Tasks

To develop basic understanding and predictive procedures for the thermal-fluidmechanical behavior of the detachment phase for metal transfer in GMA welding, preliminary approximate studies and time/length scale analyses are being applied, and numerical prediction techniques are being developed. Results will be compared to the related measurements of Prof. T.W. Eagar, MIT, and of R.A. Morris at DTRC.

The general goal and objective have been described above. The initial problem attacked is the transient behavior of the molten and solid regions for

a vertical configuration under an axisymmetric idealization. Specific tasks being attacked may be summarized as follows.

a. Conduct approximate analyses to identify the dominant phenomena in metal transfer in GMAW, for ranges of control parameters important in the automated welding of steel, super alloys, aluminum and titanium.

b. Analyze the governing equations to deduce the significant time and length scales in the problem.

c. Simplify the mathematical statement of the problem, as appropriate.

d. Develop a numerical code to predict the time-dependent thermal behavior with axial symmetry.

e. Conduct numerical predictions for conditions of experiments conducted at David Taylor Research Center, with flow visualization equipment from Idaho National Engineering Laboratory, and at MIT.

1.4 Prior studies at Westinghouse Naval Systems Division/Newport, RI

The initial attack on the tasks above was conducted on this project primarily during Winter 1988 at Gould Ocean Systems Division and then Westinghouse Oceanic Division, Newport, (RI) Facility (same group as present, but earlier "ownership"). Results and status were presented in a report by McEligot and Uhlman [1988] which included a discussion of droplet phenomena and the general problem, a review of related work, preliminary time scales analyses and approximate analyses and an introductory discussion of the anticipated

numerical technique. Essentially, tasks (a), (b) and (c) were attacked and task (d) was initiated.

A combined analytical and numerical study of droplet detachment in gas metal arc welding was initiated. Globular and spray modes were considered, concentrating on 1.6 mm (1/16 in) diameter steel wires as in the classic experimental papers of Lesnewich [1958]. Previous investigations had shown that gravitational forces and surface tension forces dominate in the globular mode with electromagnetic forces also becoming important for spray transfer.

For practical GMAW conditions, approximate analyses have been conducted, appropriate non-dimensional parameters have been calculated and time scales have been estimated [McEligot and Uhlman, 1988; also Table 2.1, Appendix A, of present report]. These efforts have been aimed at determining which simplications can be made to reduce the general governing equations (Figure 1.1) to more tractable form. Vertical alignment has been considered so the idealized problem is two-dimensional and unsteady rather than three-dimensional and unsteady. Typical time scales estimates for 1/16 inch diameter steel are about (in milliseconds):

	Globular	Spray
Droplet detachment period	50-70	2-3
Current oscillations (360, 120, 60 Hz)	3, 8, 16	3, 8, 16
Thermal conduction	300	20
Thermal surface layer	50	3
Viscous diffusion	2500	400
Thermocapillary (Marangoni)	2-60	0.3-20
Electrical conduction	$<10^{-12}$	$<10^{-12}$

The time scales estimates showed that viscous effects are expected to be unimportant unless Marangoni (thermocapillary) convention is significant. As shown in the table above, the estimate for Marangoni convection is highly uncertain in this application. As a consequence of these studies, none of the thermalfluid phenomena could be eliminated immediately, but a one-dimensional approximation should give reasonable results if the surface layer aspects are treated adequately (or if they are negligible).

Approximate values of non-dimensional parameters showed surface tension to be important - as was known. Time scales analyses indicated that convection induced by thermocapillary action ("Marangoni convection") may be significant, but that natural convection within the drop was not likely to be. Surface oscillations and power supply frequencies were seen to be comparable to the frequencies of droplet detachment; if their related amplitudes are large enough, these phenomena could contribute to scatter in droplet volumes and periods measured in experiments. Convective heat transfer to the shielding gas was found to be a quasi-steady situation for globular transfer but non-steady for the spray mode. The time scales analyses and approximate analyses did not reveal any significant simplifications to the partial differential thermofluid equations describing the general problem.

Development of a numerical code was started to treat the general problem of axisymmetric droplet detachment. The approach is comparable to the versatile TEAM code of UMIST with the additional complexities of free surfaces and continuously varying grids, phase change and transient phenomena. The TEAM [Huang and Leschziner, 1983] and VADUCT-E [McEligot and Cole, 1987; Loizou and Launder, 1987; McEligot et al., 1988] codes were used for guidance.

The numerical representation uses a finite control volume technique with finite time steps to approximate the non-steady governing equations. Axisymmetric orthogonal coordinates are employed, but a non-orthogonal mesh scheme is to be used to follow the development of the droplet and its free surface [Uhlman, 1988]. The code is being developed in stages so its components can be verified by comparison to classical analyses and experiments. The current stage treats the solution of the coupled momentum and continuity equations for liquid droplet flow as from a tube (which corresponds to the solid wire); this stage includes the complications of a variably-spaced non-orthogonal grid, transient flow and the free surface, with gravitatioal and surface tension forces corresponding to globular transfer. Geometric variables and parameters have been coded and the line-by-line, TDMA solution algorithm has been programmed. Convection terms for the momentum equations have been derived and coded; derivation of diffusion terms and diffusion source terms was initiated.

1.5 Conspectus

The present report summarizes the highlights of the studies under the current one year contract. Completed work is presented in detail primarily in the Appendices while ongoing efforts, mostly on droplet formation, are included in the body of the report.

The next section describes the current approach (very) briefly and then results for thermal conduction in the moving solid electrode are summarized in section 3. Section 4 treats the numerical prediction of droplet formation and detachment in moderate detail. A few concluding remarks complete the body of the report. Two appendices cover numerical and analytical treatment,

respectively, for the moving solid electrode; the first combines the work of Kim and Eagar with our results from the previous half-year contract [McEligot and Uhlman, 1988] and the thermal conduction studies of the present year.

2. CURRENT APPROACH

A two-pronged approach is in process. Studies concentrate separately on (1) steady thermal conduction in the moving solid electrode and (2) transient droplet formation. Work continues on literature review, approximate analyses and time scale analyses as appropriate, and investigations treating moving deformable control volumes in conjunction with free surfaces for two-dimensional, transient numerical analyses. The question whether a moving grid treatment is necessary or whether an Eulerian V-O-F approach [Hirt and Nichols, 1981] would be adequate was examined briefly; it was perceived that, if Marangoni convection is important, the length scales near the free surface would be so small that a V-O-F method could miss important details. However, we have split the complicated, general problem into two idealized regions to ease physical insight into the overall problem.

Simple transient analyses show that the solid electrode can be approximated reasonably as a steady flow, steady state, thermal conduction problem except in immediate vicinity of the growing and detaching drop. Dr. J.S. Uhlman (formerly with Westinghouse Oceanic Division) has developed a classical analysis to complement the numerical predictions of Kim and Eagar (Appendix A); details are presented in Appendix B. This treatment simulates the heating due to electron condensation on the side surface of the electrode as in argon shielding of steel electrodes [Kim, 1989].

The droplet formation and detachment problem has been reduced to a one-dimensional transient treatment. It is being attacked in the following stages:

- o Momentum and continuity equations for liquid droplet flow as from a tube (simulating melting at the end of a cylindrical electrode). Includes gravity, surface tension, motion, time-varying grid and free surface deformation.

- o Thermal energy equation with resistive heat sources and boundary heating. Includes phase change simulation at $x = 0$ (interface).

- o Thermocapillary (Marangoni) convection at surface.

- o Maxwell's equations. Adds electromotive forces for body force plus electrical current distribution.

The first stage is a substantial thermofluid mechanic problem in its own right, covering the range from static, pendent drops to steady jets. Studies of the limiting cases are found in the literature, but solutions are not readily available for the intermediate problem involving transition from slowly dripping drops to streaming jets. Our work in progress is primarily attacking this problem.

3. HEAT TRANSFER IN SOLID ELECTRODE

The process of heating the metal to the melting temperature occurs in the moving solid electrode. With the exception of disturbances in the material

properties or the surroundings or in the immediate vicinity of the transient drop, the process can be idealized as axisymmetric. Therefore, the governing equation can be written

$$\rho V \frac{\partial H}{\partial x} = \frac{\partial}{\partial x}\left(k\frac{\partial T}{\partial x}\right) + \frac{1}{r}\frac{\partial}{\partial r}\left(kr\frac{\partial T}{\partial r}\right) + q_G''' \qquad (3.1)$$

where the volumetric energy source term q_G''' depends on the electrical resistivity ρ_e.

The primary heating to T_m is by resistive heating and by thermal conduction from the molten interface itself. If the electron condensation [Kim, 1989] occurs mainly at the tip and there is no significant heat transfer from the sides, then the problem can be reduced to one dimension with the governing equation as

$$\rho V \frac{dH}{dx} = \frac{d}{dx}\left(k\frac{dt}{dx}\right) + q_G''' \qquad (3.2)$$

With the properties held constant at some appropriate average values and with boundary conditions set at the end temperatues, this equation can be solved in closed form. The result is given as equation (4.6) in Appendix A.

Kim's data [1989] indicated that, as electrical current is increased in steel electrodes shielded by argon gas, there is apparently insufficient surface area at the molten tip to accomodate the rate of electron condensation needed. Consequently, the arc attaches to the cylindrical side of the electrode (Figure 3.4 in Appendix A), causing additional heating there, and converts the mathematical description to a two-dimensional problem as in equation (3.1). Kim suggests approximating this phenomenon with a surface heating source which varies in the axial direction,

$$q_s''(x) = \frac{\alpha i V_c}{\pi r_w} \cdot \frac{1}{\sigma\sqrt{2\pi}} \exp\left\{-\frac{(L-x)^2}{2\sigma^2}\right\} \qquad \text{at } r = r_w \qquad (3.3)$$

The effect of axial thermal conduction (second term in equation (3.1)) decreases as electrode velocity, and therefore Peclet number, increases as can be seen from equation 4.6 of Appendix A. With the idealization that axial conduction is neglected and again using constant, averaged properties, the governing equation (3.1) can be reduced to

$$\frac{\partial \bar{\bar{T}}}{\partial x} = \frac{1}{r} \frac{\partial}{\partial r} \left(r \frac{\partial \bar{\bar{T}}}{\partial r} \right) + \bar{q}_G \qquad (3.4)$$

where the non-dimensional quantities are as defined in Appendix B.

Equation (3.4) is linear with respect to T if q_G''' is approximated as spatially constant (or if ρ_e is a linear function of T). Therefore, one can superpose solutions for specific boundary conditions to obtain additional solutions for other (desired) boundary conditions. It is also analogous to one-dimensional, transient conduction in a cylindrical rod for which a wide variety of solutions exists [Carslaw and Jaeger, 1959; Boelter et al., 1965; Özisik, 1980]. Further, techniques have been developed to handle the comparable thermal entry problem for internal forced convection in flow inside a circular tube. Kays [1966], Reynolds [1968], Bankston and McEligot [1969] and others have demonstrated how the solution for a constant wall heat flux can be used with superposition (Duhamel's theorem) to yield predictions for a specified variation of wall heat flux.

Superposition techniques have been used by Dr. J.S. Uhlman to obtain exact closed form solutions for idealized application to moving electrodes with electron condensation on the side surfaces. The treatment is explained in detail in Appendix B. For a uniform velocity, the general solution for the radial temperature distribution is a series of Bessel functions; eigen-

values are obtained from the zeroes of the Bessel function corresponding to the surface boundary condition (t_s or $(\partial t/\partial r)_s$ specified). To obtain the basic solution for a specified surface heat flux with internal energy generation as well, he separated the temperature distribution into three components; Arpaci [1966] has described a comparable approach for the slab geometry. Uhlman applied this solution then to form the integral relation which determines the temperature distribution when the surface heating varies in the axial direction. Suitable functions should be chosen to approximate the distribution of electron condensation in order to permit easy integration.

Since electrical resistivity and thermal conductivity vary significantly with temperature for steel (see Figure 5.1 in Appendix A), numerical methods become necessary to handle the non-linear problem. Kim [1989], therefore, applied the commercial PHOENICS code for the conditions of his experiments. Examples of solutions are given in Appendix A which combines the results of his study with ours. He concluded that his numerical simulations of steel electrodes shielded by argon gas were quantitatively consistent with his hypothesis that electron condensation on the cylindrical side surface provides an additional energy source leading to formation of a taper at high electric currents (as in Figure 3.3 of Appendix A).

4. FLUID MECHANICS OF DROPLET FORMATION AND DETACHMENT

4.1 Background

The present study concentrates on a one-dimensional, approximate treatment of droplet formation and detachment for a variety of reasons. The development provides fundamental physical insight into the droplet processes

without the complicated presentation of two- and three-dimensional descriptions and still can include consideration of all the major phenomena involved. It can provide an approximate framework to investigate whether thermocapillary convection may have a significant effect. It provides a means to establish the grid for the two-dimensional problem. Since computer time for a numerical solution varies approximately as N^3 or more (where N is the number of nodes), substantial savings in computer time are possible [Uhlman, 1989], particularly where the time steps must be extremely short to resolve capillary waves. And the limiting cases are approximated reasonably well by one-dimensional analyses [Boucher and Evans, 1975; Lienhard, 1968; Adams and Roy, 1986].

4.2 General approach

The technique attempted is patterned after the philosophy of Adams and Roy [1986] for a one-dimensional numerical model of a drop-on-demand ink jet. Essentially, the continuity and momentum equations are cast in Lagrangian form coupled to one another via the interface condition at the surface of the drop, i.e., the pressure difference across the interface (in this case, the internal pressure) is given by

$$p = \sigma K = \sigma\left[\frac{1}{R_T} + \frac{1}{R_N}\right] \tag{4.1}$$

where K represents the mean curvature of the surface. Atmospheric pressure outside the droplet is taken as the datum. Dependent variables are the instantaneous local drop radius r(x,t) and instantaneous local one-dimensional velocity V(x,t). The two equations are solved for the new values of these variables after each time step and then the locations (corresponding to the

elemental control masses) are advanced as predicted by the local velocities. The new radii and their new node locations permit determination of the internal pressure distribution P(x,t) for the momentum equation via the interface condition above.

Boundary conditions are the inlet radius and velocity which correspond to the electrode radius at the melting front and the electrode feed speed, respectively. Initial conditions require values of instantaneous droplet shape r(x,0) and pointwise velocity V(x,0).

4.3 Governing equations (Prof. J.F. Foss)

Spatial variation is taken as one-dimensional in the axial or vertical direction. The LaGrangian continuity equation is derived by considering an elemental control mass which is moving relative to the "entry" position which serves as a reference point. The distance x identifies its instantaneous location, r is its local radius and Δx its thickness as shown in Figure 4.1. Conservation of mass requires

$$\frac{d}{dt} (\pi r^2 \Delta x) = 0 \qquad (4.2)$$

or

$$r^2 \frac{d(\Delta x)}{dt} + \Delta x \frac{dr^2}{dt} = 0 \qquad (4.3)$$

Since an elemental mass, whose thickness is $\Delta x(t)$ and whose center is at x at time t, can be described by the displacement of its forward $(x + \Delta x/2)$ and aft $(x - \Delta x/2)$ faces during the time step Δt, the thickness of the mass at $(t + \Delta t)$ can be expressed as

$$\Delta x(t + \Delta t) = \Delta x(t) + [V(x + \Delta x/2) - V(x - \Delta x/2)]\, \Delta t$$

or

$$\frac{d}{dt}(\Delta x) \simeq V(x + \Delta x/2) - V(x - \Delta x/2)$$

and

$$\frac{1}{\Delta x}\frac{d}{dt}(\Delta x) \simeq \frac{V(x + \Delta x/2) - V(x - \Delta x/2)}{\Delta x} \simeq \frac{\partial V}{\partial x}$$

Hence, from equation (4.3) one can write

$$\frac{1}{r^2}\frac{dr^2(x,t)}{dt} + \frac{\partial V(x,t)}{\partial x} = 0 \qquad (4.4)$$

Since the viscous time scales for the droplet are long relative to its period, we treat the flow as inviscid for a first approximation. A LaGrangian version of the momentum equation can be derived for a one-dimensional flow by treating the motion of an elemental control mass along the axis. In addition to its rate of change of momentum we consider gravity forces, body forces to allow for electromagnetic forces and pressure (or normal stresses). The resulting governing equation becomes

$$\frac{d}{dt}V = -\frac{g_c}{\rho}\frac{\partial}{\partial x}p + g + \frac{g_c f_b}{\rho} \qquad (4.5)$$

where f_b represents the body force per unit volume.

In both of these equations the derivative d( )/dt applies to fluid particles (or elemental masses) which are identified by their instantaneous distance x from the origin. In solving the equations (for example, numerically) one must keep in mind that the position x of the particle is generally moving with time. On the other hand the spatial partial derivatives ∂( )/∂x apply only to the distributions as functions of the instantaneous values of x (as implied in the definition of a partial derivative).

When V is zero and there are no additional body forces ($f_b = 0$), this momentum equation reduces to the hydrostatic equation

$$\frac{\partial}{\partial x} p = \frac{\rho g}{g_c} \tag{4.6}$$

For a static droplet, introduction of the interface condition gives the "Laplace equation" [Boucher and Evans, 1975]

$$\rho g (h - z) = g_c \sigma \left[\frac{1}{R_T} + \frac{1}{R_N} \right] \tag{4.7}$$

Here z is measured vertically upward from an origin at the bottom tip of the droplet and h is the hydrostatic head or equivalent depth of fluid at the origin. In the limit of slow motion without other body forces the instaneous droplet shape should satisfy this equation; it has been used by a number of authors to represent a limiting case of globular transfer [Greene, 1960; Ueguri, Hara and Komura, 1985].

4.4 Scales and non-dimensional parameters

The governing momentum and continuity equations can be conveniently non-dimensionalized in terms of the liquid properties. In order to be consistent with the low velocity (static) formulation in the limit, the length scaling of Boucher and Evans is chosen

$$a = \sqrt{2 g_c \sigma / (\rho g)} \tag{4.8}$$

A capillary velocity scale is defined as

$$V_c = \sqrt{\frac{g_c \sigma}{\rho a}} = \left[\frac{g g_c \sigma}{2 \rho} \right]^{1/4} \tag{4.9}$$

which leads to a capillary time scale

$$t_c = \frac{a}{V_c} = \left[\frac{8 g_c \sigma}{\rho g^3}\right]^{1/4} \tag{4.10}$$

For liquid steel these capillary scales have values of the order of 1/2 inch, 400 in/min and 30 ms, respectively.

Non-dimensional variables may be defined as

$$\bar{r} = \frac{r}{a}, \qquad \bar{V} = \frac{V}{V_c} \qquad \text{and} \qquad \bar{t} = \frac{t}{t_c} \tag{4.11}$$

Thus the typical boundary conditions at $\bar{t} = 0$ become $\bar{r} = r_w/a$ or r_{in}/a and $\bar{V}_{in} = V_w/V_c$. For 1/16 in (1.6 mm) diameter steel wire moving at 200 in/min these values become $\bar{r}_w \simeq 0.14$ and $\bar{V}_{in} \simeq 1/2$.

Additional familiar non-dimensional parameters are employed to describe vertical liquid jets subjected to gravity [Lienhard, 1968]. The Froude and Weber numbers can be written

$$Fr = \frac{V_{in}^2}{g d_w} = \frac{\bar{V}_{in}^2}{4\bar{r}_w} \tag{4.12}$$

$$We = \frac{\rho V_{in}^2 d_w}{g_c s} = 2\bar{r}_w \bar{V}_{in}^2 \tag{4.13}$$

One expects that if the inlet or wire velocity is much greater than the characteristic capillary velocity scale, droplets will not form and a liquid jet will evolve instead. Pimbley [1976] used this reasoning to derive a criterion for the formation of a (streaming) liquid jet. In his terms, if

$\varepsilon^2 \tilde{>} 1/2$ no jet would form and with $\varepsilon^2 \tilde{<} 1/2$ one could; ε^2 is defined as

$$\varepsilon^2 = \frac{g_c \sigma}{2\rho r_o V_o^2} \tag{4.14}$$

Converted to our definitions above, his criterion becomes

$$\bar{V}_{in}^2 \cdot \bar{r}_w = (We/2) \hat{>} 1 \quad \text{(for jet)} \tag{4.15}$$

The jet may then break down into droplets at a greater distance from the inlet by capillary or Rayleigh instability as in ink jet printing [Rayleigh, 1878; McCarthy and Molloy, 1974; Pimbley, 1976; Heinzl and Hertz, 1985].

In GMA Welding typical ranges of parameters include wire diameters from 1/32 to 3/32 in. (0.8 to 2 mm) in diameter and electrode feed speeds of the order 100 to 400 in/min (0.04 to 0.2 m/sec) for globular and spray transfer modes [Eagar, 1987]. However, speeds of the order of 900 in/min may be employed for high current welding in a rotating, streaming mode [Morris, 1989]. The lower values give $\bar{V}_{in}^2 \bar{r}_w \simeq 0.1$, corresponding to the formation of individual drops before detachment. On the other hand, Kim and Eagar [Gatlinburg, 1989] report observations of steel electrodes in argon shielding where a sharp taper and molten liquid film formed above the solid tip at high electrical currents. In their case, the appropriate inlet velocity would be higher than the wire feed speed as illustrated in Figure 4.2b. Using the equation for conservation of mass for steady flow, one obtains

$$V_{in}^2 r_{in} = (V_w^2 r_w)_{solid} \cdot (r_w/r_{in})^3$$

That is, a reduction in diameter by a factor of two will lead to an eight-fold increase in $\bar{V}_{in}^2 \bar{r}_{in}$. In Figure 4.4(e) of Kim's thesis [1989] one can estimate a reduction by a factor of eight for a 1/16 in. steel electrode,

so that $\bar{V}_{in}\bar{r}_{in}$ would be well above unity and a streaming liquid jet would be expected.

Thus, the thermofluidmechanic range of interest for metal transfer is expected to range from quasi-static liquid droplets ($V_w r_w \ll 1$) to "steady" jets ($\bar{V}_{in} r_{in} \gg 1$). It is desireable that the numerical analysis be capable of treating this entire range. The general approach of Adams and Roy shows promise of accomplishing this objective and so it is attempted here.

4.5 Non-dimensional problem statement

Substitution of the scales defined in the previous section allows writing the governing equations as

Continuity

$$\frac{1}{\bar{r}^2}\frac{d\bar{r}^2}{d\bar{t}} + \frac{\partial}{\partial\bar{x}}\bar{V} = 0 \tag{4.16}$$

Momentum

$$\frac{d\bar{V}}{d\bar{t}} + \frac{\partial}{\partial\bar{x}}(\bar{p}) - 2(1 + \bar{f}_b) = 0 \tag{4.17}$$

where non-dimensional pressure is defined as $p = a\bar{p}/\sigma_r$ and σ_r is the surface tension evaluated at an appropriate reference temperature (e.g., T_{melt}). The auxiliary condition relating $\bar{p}(\bar{x})$ to $\bar{r}(\bar{x})$ at an instant becomes

$$\bar{p} = \bar{\sigma}\left\{\frac{1}{\bar{R}_T} + \frac{1}{\bar{R}_N}\right\} \tag{4.18}$$

where $\bar{\sigma} = \sigma/\sigma_r$ and $\bar{R}_T$ and $\bar{R}_N$ are the non-dimensional transverse (profile) and and normal (circumferential) radii of curvature of $\bar{r}(\bar{x})$. The surface tension σ is permitted to vary spatially for later coupling to the solution of a thermal energy equation. At the lower tip of the drop ($z = 0$), rotational symmetry requires $R_T = R_N$.

As presented, both governing equations are first order partial differential equations with x and t as independent variables . The location x(t) of an individual fluid particle may be described by the cumulative steps which have occurred since the initiation of the motion. Specifically, from time j to j + 1, the fluid mass translates as

$$x(t_{j+1}) \simeq x(t_j) + V(x(t_j), t_j)\, \Delta t_j$$

where Δt is the time step used to describe the problem and the Eulerian description of the velocity, V(x,t), is used to define the transport of the identified mass. For unique solutions, boundary and initial conditions must be prescribed. Appropriate boundary conditions are (1) $\bar{V}(0,t)$ = constant or specified fn(t) and (2) $\bar{r}(0,t) = \bar{r}_w$ or $\bar{r}_{in}$. Initial conditions should be some realizable spatial functions $\bar{V}(\bar{x}_i,0)$ and $\bar{r}(x_i,0)$. For the first attempts at solution the initial shape is taken as an arc of a circle with $\bar{r}(0,0) = \bar{r}_w$ and the initial velocity distribution is taken as uniform at $\bar{V}(x,0) = \bar{V}_{in}$ = constant.

4.6 Method of solution

In the rest of this chapter the overbars denoting non-dimensional variables are suppressed except where required for clarity, i.e., the quantities are considered as non-dimensional.

Numerical methods are applied to solve the mathematical problem stated in the previous section. In general, the approach of Adams and Roy [1986] is followed where applicable. Since our first attempt is treated as inviscid, the techniques are not exactly identical; differences in detail also exist since their computer code is considered proprietary and is not available to the general public.

After setting the initial profiles of r(x,0) and V(x,0), a marching solution is conducted in time. Input control parameters are material properties, electrode feed speed and electrode diameter as well as normalized values for the acceleration of gravity and other body forces ($f_b = 0$ usually). These quantities are applied to calculate the non-dimensional variables and control parameters. Additional input includes a value of $\bar{H} = h/a$ for setting the initial profile plus various numerical and printing control parameters.

To set initial conditions, the initial profile r(x,0) is taken as the arc of a circle which passes through r_w, corresponding to a spherical segment of one base [Burington, 1948]. For a constant radius of curvature (as in a circle) the height of that segment is given as

$$z_e = [1 - \cos(\Theta/2]/H \tag{4.19}$$

where $\Theta = 2 \sin(r_w \cdot H)$. The height z_e is divided into M-1 elements Δx_i, uniform except for a couple near the tip of the drop. Locations x_i and $z_i = z_e - x_i$ are calculated in the process and the radii at these nodes are determined from

$$r_i = (1/H) \sqrt{1 - (1 - z_i H)^2} \tag{4.20}$$

since the radius of curvature of the circle is $R_o = 1/H$. Initial velocities are set at V_i or $V(x_i) = V_{in}$ and for now σ_i is taken as unity.

Initial (and later) time steps are taken as a factor (called TCONTR)

times the lesser of the Courant-Friedrich-Loewy criterion [Roache, 1982]

$$\Delta t < \Delta x_i / V_i$$

or a criterion for resolution of capillary waves [Foote, 1973; Adams and Roy, 1986]

$$\Delta t < \frac{2}{3\sqrt{\pi}} \Delta x_i^{3/2}$$

Typical values of z_e were about $r_w/3$ so, even with a coarse grid (M = 10), the latter criterion generally dominated for conditions of interest in GMA welding.

As done by Adams and Roy, the continuity equation is rephrased as

$$\frac{d \ln r^2}{dt} + \frac{\partial V}{\partial x} = 0$$

or

$$\frac{d (2 \ln r)}{dt} + \frac{\partial V}{\partial x} = 0 \qquad (4.21)$$

The two governing equations are then written in vector form as

$$\frac{d\underline{U}}{dt} + \frac{\partial \underline{F}}{\partial x} + \underline{G} = 0 \qquad (4.22)$$

with components

$$U_r = 2 \ln r \ , \qquad F_r = V \ , \qquad G_r = 0$$

and

$$U_V = V \ , \qquad F_V = p \ , \qquad G_V = -2(1 + f_b)$$

A crude finite difference approximation to the change during a time step would then be $\Delta \underline{U} \simeq - \Delta t[\Delta \underline{F}/\Delta x) + \underline{G}]$.

DMM/ld/0559m

In order to determine the curvature terms in the auxiliary interface relation for the pressure, the surface profile is parameterized in terms of arc length s along the surface from the tip at i = M (z = 0) [Brazier-Smith, Jennings and Latham, 1971]. This procedure is employed to constrain the necessary spatial derivatives to reasonable values [Uhlman, 1989]. A group of spline and differentiation subroutines were developed by Uhlman earlier [1982].

In terms of axial position z(s) and radius y(s), the required curvature terms for p(x) can be written

$$\frac{1}{R_T} = \frac{d\phi}{ds} = \frac{dy}{ds} \cdot \frac{d^2z}{ds^2} - \frac{dz}{ds} \cdot \frac{d^2y}{ds^2} \qquad (4.23)$$

and

$$\frac{1}{R_N} = \frac{\sin \phi}{y} = \frac{1}{y} \cdot \frac{dz}{ds} \qquad (4.24) .$$

where ϕ is the angle measured from the horizontal as done by Boucher and Evans [1975]. (Uhlman [1989] has provided a derivation of $1/R_T$ in terms of Θ, the complement of ϕ so his result differs by a change of sign.) At z = 0, $R_T = R_N = 1/(d^2z/ds^2)$ by symmetry.

The procedure for determining p(x) follows. The radius r is calculated from $\underline{U}_r = 2 \ln r$ and is identified (also) as y for y(z). Subroutine AXIDK calculates s_i by spline fitting via the pairs y_i, z_i, starting at the nose where dy/ds = 1 and dz/ds = 0. The coefficients for the spline function representations of y(s) and z(s) are also stored. Subroutine DRIVDK is applied at s_i to determine dy/ds and d^2y/ds^2 at these locations from the stored coefficients. It is then applied again to obtain dz/ds and

d^2z/ds^2 from z(s). The derivatives are substituted in the relations above for $1/R_T$ and $1/R_N$ and $p(x_i)$ is determined from

$$p = \sigma[(1/R_T) + (1/R_N)] \tag{4.25}$$

At each time step a predictor-corrector calculation, patterned after the MacCormack approach [Roache, 1982; Adams and Roy, 1986], is applied to determine the new radii and velocities corresponding to the locations x_i at the start of the time step. The sequence is

a) Apply spline fit and differentiation to $r(x_i)$ to determine $p(x_i)$

b) Apply forward spatial differencing from i = 2 to i = M-1 to obtain predicted values of ln $r(x_i)$ and $V(x_i)$ for the new time (but still related to old x_i)

c) Determine values for end point (tip) at i = M

d) Obtain predicted values of $p(x_i)$ from predicted $r(x_i)$ via spline fit and differentiation.

e) Apply backward spatial differencing from i = M-1 to i = 2 to calculate "corrected" estimates of ln $r(x_i)$ and $V(x_i)$ for the new time still related to old x_i)

f) (Sometimes) recalculate the tip estimates at i = M

The new locations of the nodes (elemental masses) are then determined by translation

$$x_i^{k+1} = x_i^k + (1/2) \cdot (V_i^k + V_i^{k+1}) \cdot \Delta t$$

and the sequence can start again for the following time step.

Several approaches have been used for calculation of conditions at the last node corresponding to the elemental mass for the tip ($z = 0$ or $i = M$). Adams and Roy apparently simply assign $V_M = V_{M-1}$ to advance this point and recognize that $r_M = 0$. In their case (without gravity) this treatment probably infers negligible viscous effects and "plug flow" in that region, which in turn implies uniform pressure and a spherical shape with constant radius of curvature ($r''_{M-1} = r''_M = 1/R_T = 1/R_N$). In our situation, F_g (and/or F_b) should modify p(x) between M and M-1 even if $V_M = V_{M-1}$; the difference would appear in F_σ which will often dominate.

Our current attempt for the tip treatment applies the momentum equation for the predictor calculation and relocates x_M temporarily. The pressure is calculated as $p_M = 2\sigma_M(d^2z/ds^2)_M$ and the predicted r_M is reset to zero. Then the predicted value of V_M is calculated directly from the momentum equation with forward spatial differencing; the interpretation is that this equation applies within the droplet up to the infinitesmal interface. To correspond to the prediction of r_i for all other nodes a predicted new value of x_M is estimated relative to x_{M-1} by applying conservation of mass to a spherical segment of one base. The relationship derived is

$$\Delta(x_M - x_{M-1}) \simeq \frac{2(V_{M-1} - V_M)\,\Delta t}{1 + \left| (x_M - x_{M-1})/r_{M-1} \right|^{2/3}} \qquad (4.26)$$

which is added to x_M to give a value corresponding to r_M that is comparable to the revised values of r_i. The new x_M is used to relocate the values z_i (i.e., $x_M - x_i$) before repeating the spline fitting of r(z) to determine $p(x_i)$ for the corrector sweep. (There is an operational question here on what is the best way of evaluating $\partial p/\partial x$ relative to the timing of time step, e.g., should p_i be recalculated for the corrector sweep without resetting all x_i as well as r_i?)

After completion of the backward-differencing corrector sweep, the tip velocity V_M is recalculated from the predicted $p(x_i)$ but by forward spatial differencing, since there is no location M+1 to use in a backward difference. As with the other quantities, the corrected value is taken as the average of the two calculations. The process for calculating a revised Δx_M is repeated and it, too, is averaged with the previous prediction to give a corrected x_M. This calculation completes the process for a time step before the locations x_i are translated for the next step. The location of the tip x_M is then translated by its estimated velocity as are the rest.

An additional node is added when the distance $x_2 - x_1$ becomes too large; then a regridding procedure is applied to redistribute the nodes more evenly. Regridding is also accomplished at fixed time intervals in an attempt to avoid difficulties caused by excessively short or large distances between nodes [Daly, 1969]. A subroutine REGRID is called to reapportion the locations x_i with the spline fitting routines as follows. Subroutine AXIDK is applied again to determine the coefficients for y(s) and z(s) from the results of r(x) of the last step. New approximate locations x_i are chosen. End points x_1 and x_M

(z_1 and z_M) remain fixed. Subroutine UGLYDK forms the coefficients for s(z) and subroutine EVALDK then is used to pick s_i from the approximate new z_i. These values s_i are used with EVALDK applied to the coefficients for y(s) and z(s) to obtain the new interpolated values of r_i and x_i that are actually adopted. The function V(s) is also deduced via subroutine UGLYDK from the original V_i and s_i; it is then employed with EVALDK to yield interpolated values of V_i at the new s_i (and, therefore, at the new z_i).

The criterion for adding a node is that the elapsed time (since adding the last node) corresponds to axial displacement of inlet particles by a specified fraction of the inlet radius. Any regridding is accomplished after the translation of the nodes to new locations x_i. After the regridding, the time interval for the next step is calculated from the criteria mentioned above and the sequence returns to the next predictor step with calculation of $p(r_i(x_i))$ for the new x_i. The procedure is terminated when the total elapsed time or the number of time steps exceeds a value which may be specified in the input file (or when a run time error occurs).

4.7 Initial results

The first calculations have been conducted with properties approximating steel, $\rho \approx 500$ lbm/ft^3 and $\sigma \approx 0.08$ lbf/ft, at earth's gravity and no additional body forces. Thus globular transfer would be simulated. "Electrode" diameter has been 1/16 in. with feed speeds of 100 and 200 in/min, plus a few at 5200 in/min to correspond to the non-dimensional parameters of the ink jets of Adams and Roy [1986]. These properties give scales of $a \approx 0.21$ in, $V_c \approx 390$ in/min and $t_c \approx 33$ ms. For $V_w = 200$ in/min and these properties and diameter, the non-dimensional parameters become $r_w \approx 0.14$, $V_{in} \approx 0.52$, $We \approx 0.075$, $Fr \approx 0.48$ and $\epsilon^2 \approx 13$, corresponding to drop formation rather than a jet.

The initial profile has been derived for $H = 5$ which gives $z_e \approx 0.057$ with

this value of r_w. A coarse initial grid of M = 10 or 20 has been employed for debugging to reduce computer run time. At early time, the (non-dimensional) time step criteria give constraints of the order of $\Delta t < 1 \times 10^{-3}$ from Courant, Friedrich and Loewy and $\Delta t < 3 \times 10^{-4}$ for capillary waves. By comparison the non-dimensional period is P ≃ 2 for globular transfer. The resulting initial shape is as shown in Figure 4.3a. An example of the pressure profile after a few steps is given as Figure 4.4.

Calculations to date have been hampered by problems which might loosely be termed numerical instabilities of which Figure 4.3 is an example. This sequence was done with TCONTR = 0.33 so the time steps were held to one-third of the applicable criterion (capillary waves) but no redistributin of nodes was employed. At time step N = 201 (t ≃ 0.007) a slight oscillation is evidently superposed on the general shape r(x). During the next 200 steps the minimum value of Δx becomes successively smaller so the time step criterion becomes more constraining, reducing to $\Delta t \simeq 10^{-6}$ by N = 400. Consequently, time advances only from t ≃ 0.007 to t ≃ 0.008 on doubling the number of steps. Meanwhile, the oscillation becomes much more exaggerated and the appearance at the tip becomes unrealistic. Regridding every 10 or 50 time steps eases the problem of small time steps but significant oscillations still appear as the droplet forms (particularly near the tip) and evolve into negative radii, overlapping nodes and comparable numerical difficulties which halt the calculation.

4.8 Next steps

Efforts continue to develop a more "robust" calculation procedure without adopting the full two-dimensional confined two-fluid technique of Daly [1969] which might be considered to be an approach held in reserve. As implied in section 4.6 other options exist for treating the tip element and the sequence of the pressure calculation.

Flows with free surfaces and significant surface tension are known to have a wide variety of interesting and beautiful behavior (as is evidenced by many of the transient drops, jets and related patterns appearing in television commercials), partly due to sensitivity to instabilities. For example, Taylor [1964] recounted how a slight variation in the aspect ratio or vertex angle of an ellipsoidal drop in an electric field can lead to issuing a very narrow axial jet from the drop. Therefore, it is appropriate to re-examine and perhaps revise the initial profile. Another logical starting point would be a profile based on the shape of the pendent drop [Boucher and Evans, 1975] of depth z_e and radius r_w instead of a spherical segment through these points. A more gradual initiation to V_{in} may be desireable as well, perhaps a linear increase from zero velocity to the desired value.

It is known that viscous diffusion terms can help stabilize numerical calculations [Richtmyer, 1957]. While the time scales estimates indicate that the current problem is approximately inviscid, it may be useful to add viscosity to the simulation. Professor Foss of Michigan State is presently developing a one-dimensional treatment of the viscous effects for inclusion in the viscous momentum equation as by Adams and Roy [1986]. It will be added (to equation (4.5) and F_v) if these other approaches do not satisfactorily resolve the difficulties. For a general treatment viscous effects are necessary to provide a damping mechanism so that an ultimate steady state is possible for a disturbed pendent drop (not necessarily in GMA welding).

4.9 Two-dimensional computational modelling of hydrodynamic droplet processes

(Prof. B.E. Launder and Dr. M.A. Leschziner, UMIST)

An analysis designed to yield information on local rather than global

droplet properties must necessarily be based on the partial differential equations governing mass, momentum and energy conservation. Even for laminar conditions, the equations are non-linear and coupled in a way which demands, for non-trivial geometries, a numerical approach to be adopted.

With heat/species transfer and electro-magnetic features left aside, a general hydrodynamic simulation of droplet formation and growth involves two main issues:

- o motion within a given droplet/electrode surface;
- o temporal adjusment of droplet surface

4.9.1 In-droplet motion On the assumption that the droplet and the processes within it are axisymmetric, the droplet must be covered by a two-dimensional numerical mesh. The type of mesh chosen is of considerable importance to the accuracy, economy, flexibility and algorithmic complexity of the numerical solution procedure. In present circumstances, the number of sensible mesh-type options is small. Clearly, a surface-adapted, hence curvilinear, mesh is required if near-surface processes are to be captured accurately and boundary conditions are to be imposed properly. Such a grid may be orthogonal or non-orthogonal. The former is preferable on grounds of mesh smoothness, level of solution error arising from grid skewness and simplicity of the discretised transport equations. However, an orthogonal mesh offers little flexibility in respect of mesh control and demands a numerical solution of a set of Poisson equations governing the mesh-line coordinates within the solution domain. Ordinarily, the cost of the mesh-generation process is marginal, for the mesh is only generated once. Here, however, the mesh is to be adapted to a time-varying solution domain, and CPU costs rise rapidly.

Thus, an algebraically generated non-orthogonal grid is a clearly preferable alternative. Such a mesh is easily adapted to a moving surface at low cost, and allows a high degree of mesh control to be exercised. The penalties paid are loss of grid smoothness, grid skewness and a considerable complication of the discretisation process which must start from the differential equations expressed in terms of general non-orthogonal coordinates.

Within the above non-orthogonal framework, the equations may be expressed in a varity of forms: in strongly-, weakly- or non-conservative form, in terms of co-variant, contra-variant or Cartesian velocity components, etc. Here again, the choice will have a considerable impact on the properties of the numerical algorithm. Current trends are towards adopting, particularly for complex 3D internal flows, a "middle-of-the-road" approach involving a Cartesian velocity decomposition within a conservative finite-volume framework (see the review by Leschziner [1989]). A distinct advantage arising from a retention of the Cartesian decomposition is that all transport equations, whether governing a scalar property or any component of a vectorial or tensorial flow property, are of the same form.

Given the typical range of Reynolds number encountered in droplets arising in GMA welding is seems highly probable that the flow within the droplet will be non-turbulent. This view is reinforced by the fact that envisioned circulation patterns of the liquid metal within the droplet will tend to stabilize flow disturbances. Thus, assuming diffusion processes (if significant) to be viscous and Newtonian and referring to the quantities defined in Figure 4.5, the governing equation for any two-dimensional (axisymmetric) flow may be written:

$$\frac{\partial}{\partial t}\rho r\phi + \frac{\partial}{\partial x_1}(C_{1\phi} + D_{1\phi}) + \frac{\partial}{\partial x_2}(C_{2\phi} + D_{2\phi}) = JrS_\phi$$

where C, D and S relate, respectively, to convection and diffusion and source; all are defined in Table 4.1, as is the Jacobian J.

Discretisation is most frequently and conveniently performed by integrating the above equations over finite-volumes of the type shown in Figure 4.6. Conventional algorithms, mainly for Cartesian grids, involve 3 sets of mutually staggered volumes, two pertaining to the momentum components and the third used to satisfy conservation of mass and scalar properties. This approach avoids numerially destabilising chequerboard oscillations but is complex, particularly for 3D situations. However, a recent proposal by Rhie and Chow [1983] now allows a collocated (non-staggered) arrangemnt to be adopted without stability problems, and most non-orthogonal-mesh schemes have adopted this route.

Examples of 2D flows computed by Lien and Leschziner [1989] at UMIST are shown in Figure 4.7. We draw attention to the fact that, in the computations displayed (and despite the fine mesh employed in certain regions) no difficulties were encountered in solving equations for velocity components not aligned with the rigid boundary provided by a wall. There is no reason to suppose that, in handling free surface boundaries, such as are present with droplets, the new factors present would create major obstacles to the use of non-aligned velocity components. An accurate resolution of the pressure difference across the gas/liquid interface of the droplet is, of course, essential. This pressure difference is in turn intimately connected with the surface topography of the drop, a feature that may require a highly refined mesh near the droplet surface, especially in the vicinity of the solid/liquid

boundary where spatial changes in surface curvature are likely to be rapid. Given that the model chosen is an axisymmetric one, such mesh refinement poses no insurmountable problems.

The above considerations should suffice to indicate that a hydrodynamic calculation within a defined, invariant droplet shape poses no particular problems with currently available general software.

4.9.2 Adjustment of droplet surface This might proceed on the basis of the balance of forces due to the internal pressure close to the droplet surface and the surface-tension force in the locally curved droplet surface.

Given a surface shape at an initial time level (n), one may assume that the pressure at the computational node closest to the surface, Figure 4.8, is known. It is assumed that the gas surrounding the droplet is effectively stagnant, implying negligible surface shear stress except when Marangoni convection is significant. (Alternatively, a gas stream symmetric with respect to the vertical axis of the bubble could also be accommodated within the proposed framework.)

During the computational interval Δt, i.e., (n) to (n+1), both near-surface pressure and the entire cross-droplet grid would be held temporarily invariant. A hydrodynamic cycle (iteration) would then yield a new velocity and internal pressure field, the latter via a pressure-correction algorithm. One outcome of this cycle would be an apparent cross-surface velocity, V_s, resulting from the supply of molten metal into the droplet from the electrode, Figure 4.9. The adjustment of the droplet would result as an outward shift of the surface by $V_s \Delta t$, and the new surface curvature distribution would give

a corrected near-surface pressure. In-step iteration could be performed to take coupling into account though this may not be necessary except, possibly, in the vicinity of drop detachment. A tangential motion within the droplet, at its surface, could in general be expected to contribute to the behaviour of the surface. This could be accommodated without difficulty.

4.9.3 Further considerations Although attention has focused on the liquid-gas interface another significant problem-determined boundary is that between the solid and liquid weld material. While in initial computations it may be convenient to take that boundary as a prescribed uniform temperature horizontal plane surface, a serious study of the droplet dynamics (at the same level as implied by the discussion under §4.9.2 demands that the interface location be determined as the computation proceeds by including the appropriate latent heat terms in the energy balance for the specially formulated set of difference equations for the control volumes contiguous with the liquid-solid interface.

Within the solid material a simple heat conduction equation (or rather the very simple convection equation involving a uniform convection velocity equal to the electrode feed speed) must be solved. Either a truncated version of the same solver used for the droplet or a separate, simpler program can be adopted.

5. CONCLUDING REMARKS

A combined analytical and numerical study of metal transfer in gas metal arc welding was continued. Globular and spray modes were considered, mostly concentrating on 1.6 mm (1/16 in) diameter steel wires as in the classic experimental papers of Lesnewich [1958]. Previous investigations have shown

that gravitational forces and surface tension forces dominate in the globular mode with electromagnetic forces also becoming important for spray transfer. Approximate analyses and time scale estimates were continued to guide the development of a general numerical technique for examining the problem and for obtaining predictions for appropriate ranges of parameters. Work also continues on the treatment of deformable control volumes in conjunction with free surfaces for two-dimensional, transient analyses.

A two-pronged approach is in process. Studies concentrate separately on (1) steady thermal conduction in the moving solid electrode and (2) transient droplet formation. Thus we have split the complicated, general problem into two idealized regions to ease physical insight into the overall process.

Simple transient analyses showed that the solid electrode can be approximated reasonably as a steady flow, steady state, thermal conduction problem except in the immediate vicinity of the growing and detaching drop. Results of the first half year study were combined with those of Kim and Eagar at M.I.T. for heat transfer in the solid electrode (Appendix A).

Axial thermal conduction in the solid electrode is primarily important only for a distance of the order of 5D/Pe from the tip where it supplies the energy necessary to supplement resistive (Joule) heating and brings the temperature to the melting point. With argon shielding of steel at high electrical currents, Kim showed that there is apparent heating of the cylindrical side surfaces due to electron condensation. Dr. J.S. Uhlman developed a closed form analysis for an idealized description of this problem. To account for the spatially-varying surface heating, he applied the method of superposition to his basic solution for uniform internal energy generation with a step change in surface heat flux

for a moving solid electrode. The approach is analogous to transient thermal conduction in an infinite cylindrical rod and to thermal entry convection problems for flow inside tubes. Though the results are only approximate, due to the idealizations necessary to set up an exact solution, they should be useful to estimate the initial location of side surface heating and to provide a means for validating most features of more general numerical analyses.

The time scales analyses identified several phenomena with thermal response of the same order-of-magnitude as the droplet period. Also, the appropriate time scales for Marangoni (thermocapillary) convection were uncertain. Therefore, in order to investigate the effects of Marangoni convection on droplet formation and detachment, one must employ a transient analysis with provision for temporal surface deformation. A steady state calculation for flow in a spherical geometry (which could be attempted with some existing general purpose programs) would be inappropriate.

For liquid steel, length, velocity and time scales were estimated to be of the order of 1/2 inch, 400 in/min and 30 ms, respectively. Appropriate non-dimensional parameters can be formed as velocity $\bar{V}_{in} = V_w/V_{cap}$, radius $\bar{r}_w = r_w/l_{cap}$, detachment period $\bar{P} = P/t_c$. The Weber number becomes $2\bar{r}_w\bar{V}_{in}^2$. If $\bar{r}_w\bar{V}_{in}^2 << 1$, capillary velocities can be expected to cause the formation of droplets, while if $\bar{r}_w\bar{V}_{in}^2 >> 1$, a "steady" jet should form (it may break up into droplets by Rayleigh instability later). The former corresponds to globular and spray conditions while the later <u>may</u> explain streaming transfer. The limiting situations of static pendent drops and of steady jets have been treated in the literature, but there is a paucity of information on the intermediate case--the transition from drops to jet with $\bar{r}_w\bar{V}_{in}^2$ near unity,

Transient numerical analyses are under development to predict the droplet formation and detachment process. With surface tension forces included, it is necessary to constrain non-dimensional time steps to $\Delta t < (2/3\sqrt{\pi})\Delta x^{3/2}$ which is of the order of 10^{-4} for coarse grids and typical conditions. Thus, one expects more than 1000 time steps between detachments for spray transfer and 20-30,000 for the globular mode. This provides an incentive for using a limited number of nodes (N) since computer time typically varies as N^3 or more.

To provide initial physical insight without the complications (and computer time) of a two-dimensional treatment, a one-dimensional transient technique is in process to describe the droplet formation and detachment. LaGrangian representations of the continuity and momentum equation have been derived for the liquid leaving the molten interface. Spline representations are used to determine surface curvature terms necessary for the liquid-gas interface condition which provides the internal pressure distribution. A predictor-corrector technique, like that of MacCormack, is applied at each time step to determine the new values of the radii and velocities of the deforming control masses to which the LaGrangian formulation applies. After revising radii and velocities, the nodes (locations of masses) are translated forwards or backwards for the start of the next time step. Several approaches have been applied for the tip of the drop but apparent numerical instabilities continue; a more robust treatment is sought. As the drop grows, additional nodes are added and the locations are redistributed; radii and velocities at the new sites are determined via spline subroutines. Once this program is calculating liquid flow reliably, from droplet to jet, plans call for addition of the energy equation to predict temperatures and a surface shear representation to treat Marangoni convection.

DMM/ld/0559m

ACKNOWLEDGEMENTS

The author and his collegues are grateful to the Office of Naval Research and their Scientific Officers, Drs. Bruce A. MacDonald, Ralph W. Judy and George R. Yoder for encouragement and for financial support from the Welding Science Program of their Material Science Division. Professor Thomas W. Eagar and Dr. Y.-S. Kim of Massachusetts Institute of Technology, Dr. James S. Uhlman, Jr., now of the Naval Underwater Systems Center, Professor John F. Foss of Michigan State University and Professor Brian E. Launder and Dr. Michael A. Leschziner of the University of Manchester Institute of Science and Technology all provided substantial collaboration, guidance and insight for which the Principal Investigator is most appreciative. Parts of Appendix A were accomplished under financial support from the Department of Energy to Professor Eagar at Massachusetts Institute of Technology. We also thank Mssrs. Richard A. Morris and Robert R. Hardy of the David Taylor Research Center for continuous interest and advice. And Mrs. Eileen Desrosiers is to be applauded for excellent typing in a very compressed and demanding time scale.

DMH/ld/0559m

General Transport Equation: $\frac{\partial}{\partial x_1}\{C_{1\phi}\,\phi + D_{1\phi}\} + \frac{\partial}{\partial x_2}\{C_{2\phi}\,\phi + D_{2\phi}\} = J\,S_\phi\,r$

ϕ	$C_{1\phi}$	$C_{2\phi}$	$D_{1\phi}$	$D_{2\phi}$	S_ϕ
1	$U_1 r$	$U_2 r$	0	0	0
v_1	$U_1 r$	$U_2 r$	$-\frac{\mu r}{J}\left\{\beta_1^1\frac{\partial v_1}{\partial x_1} + \beta_2^1\frac{\partial v_1}{\partial x_2} + \beta_1^1\omega_1^1 + \beta_2^1\omega_1^2\right\}$	$-\frac{\mu r}{J}\left\{\beta_1^2\frac{\partial v_1}{\partial x_1} + \beta_2^2\frac{\partial v_1}{\partial x_2} + \beta_1^2\omega_1^1 + \beta_2^2\omega_1^2\right\}$	$-\frac{1}{J}\left\{\frac{\partial}{\partial x_1}\{p\beta_1^1\} + \frac{\partial}{\partial x_2}\{p\beta_1^2\}\right\}$
v_2	$U_1 r$	$U_2 r$	$-\frac{\mu r}{J}\left\{\beta_1^1\frac{\partial v_2}{\partial x_1} + \beta_2^1\frac{\partial v_2}{\partial x_2} + \beta_1^1\omega_2^1 + \beta_2^1\omega_2^2\right\}$	$-\frac{\mu r}{J}\left\{\beta_1^2\frac{\partial v_2}{\partial x_1} + \beta_2^2\frac{\partial v_2}{\partial x_2} + \beta_1^2\omega_2^1 + \beta_2^2\omega_2^2\right\}$	Plane: $-\frac{1}{J}\left\{\frac{\partial}{\partial x_1}\{p\beta_2^1\} + \frac{\partial}{\partial x_2}\{p\beta_2^2\}\right\}$ Axisymmetric: $S_\phi = S_\phi - 2\mu\frac{v_2}{r^2}$
ϕ	$U_1 r$	$U_2 r$	$-\frac{\mu r}{J\sigma_\phi}\left\{\beta_1^1\frac{\partial\phi}{\partial x_1} + \beta_2^1\frac{\partial\phi}{\partial x_2}\right\}$	$-\frac{\mu r}{J\sigma_\phi}\left\{\beta_1^2\frac{\partial\phi}{\partial x_1} + \beta_2^2\frac{\partial\phi}{\partial x_2}\right\}$	0 $-\rho g$

where,

$r = 1$ for plane flows

β_j^i = cofactor of $\frac{\partial y_i}{\partial x_j}$ in J

$$J = \begin{vmatrix} \frac{\partial y_1}{\partial x_1} & \frac{\partial y_2}{\partial x_1} \\ \frac{\partial y_1}{\partial x_2} & \frac{\partial y_2}{\partial x_2} \end{vmatrix}$$

$B_j^i = \beta_1^i\beta_1^j + \beta_2^i\beta_2^j$, $\omega_j^i = \frac{\partial v_i}{\partial x_1}\beta_j^1 + \frac{\partial v_i}{\partial x_2}\beta_j^2$

$U_1 = \rho\cdot(v_1\beta_1^1 + v_2\beta_2^1)$, $U_2 = \rho\cdot(v_1\beta_1^2 + v_2\beta_2^2)$

Table 4.1 C,D and S terms for individual equations

Governing Equations

Momentum

$$\rho \frac{D\vec{u}}{Dt} = -\nabla p + \rho\vec{g} + (\nabla \times \vec{H}) + \mu_m \vec{H} + q\vec{E} + \mu\nabla^2\vec{u}$$

Thermal Energy

$$\rho C_p \frac{DT}{Dt} = \nabla \cdot (k\nabla T) + \frac{\mu}{2}(\nabla\vec{u} + \nabla\vec{u}^{\bullet})^2$$

Species (additives)

$$\frac{DC}{Dt} = K_s \nabla^2 C$$

Continuity

$$\nabla \cdot \vec{u} = 0$$

Maxwell's Equations

$$\nabla \times \vec{E} = -\frac{\partial}{\partial t}(\mu_m \vec{H})$$

$$\nabla \times \vec{H} = \sigma(\vec{E} + \vec{u} \times \mu_m \vec{H})$$

and Property Relations

plus Interface/Boundary Conditions

FIGURE 1.1 General system of partial differential equations governing droplet formation and detachment.

DHM/ld/0559m

Typical Boundary Conditions

Liquid Metal Surface

Energy Balance between

- Conduction
- Convection
- Radiation
- Energy Absorbed from Plasma Arc
- Energy Required for Vaporization

Force Balances accounting for

- Surface Tension with Surface Curvature
- Pressure Differences
- Drag of Shielding Gases

Specified **distributions** of **magnetic** and **electric fields**

Balance of **mass** fluxes of individual **species**

FIGURE 1.1 Continued.

DMM/ld/0559m

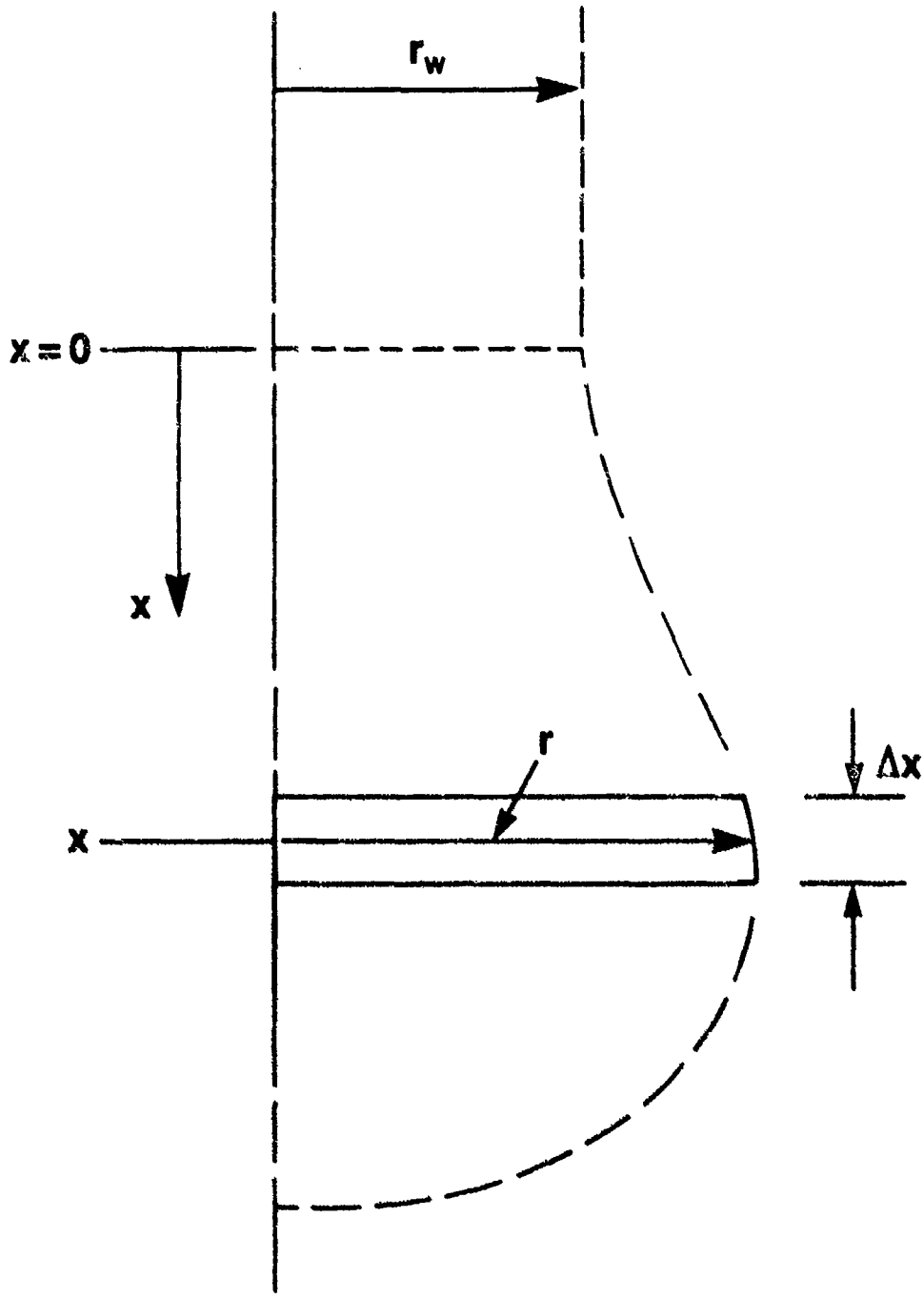

Figure 4.1. Elemental control mass for derivation of continuity equation.

DMM/ld/0559m

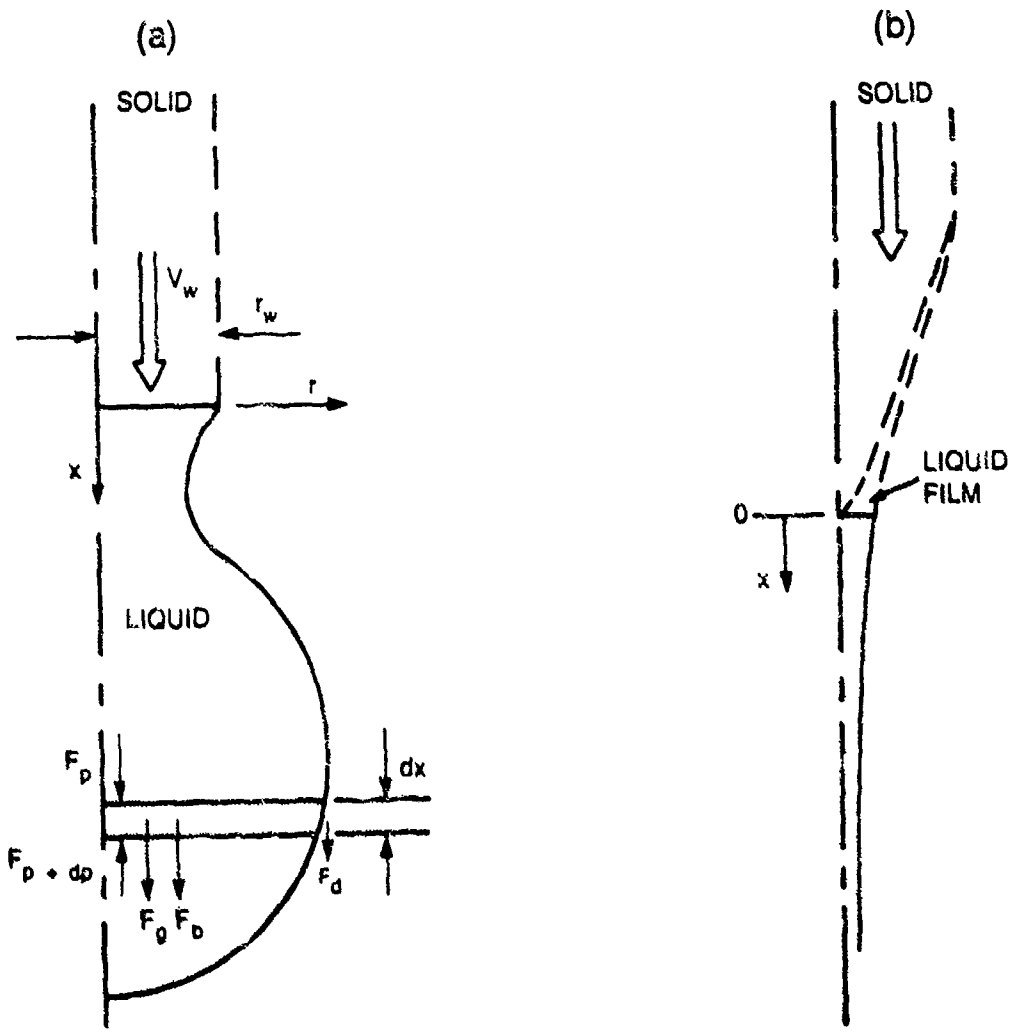

Figure 4.2. Limiting situations considered.

DMM/ld/0559m

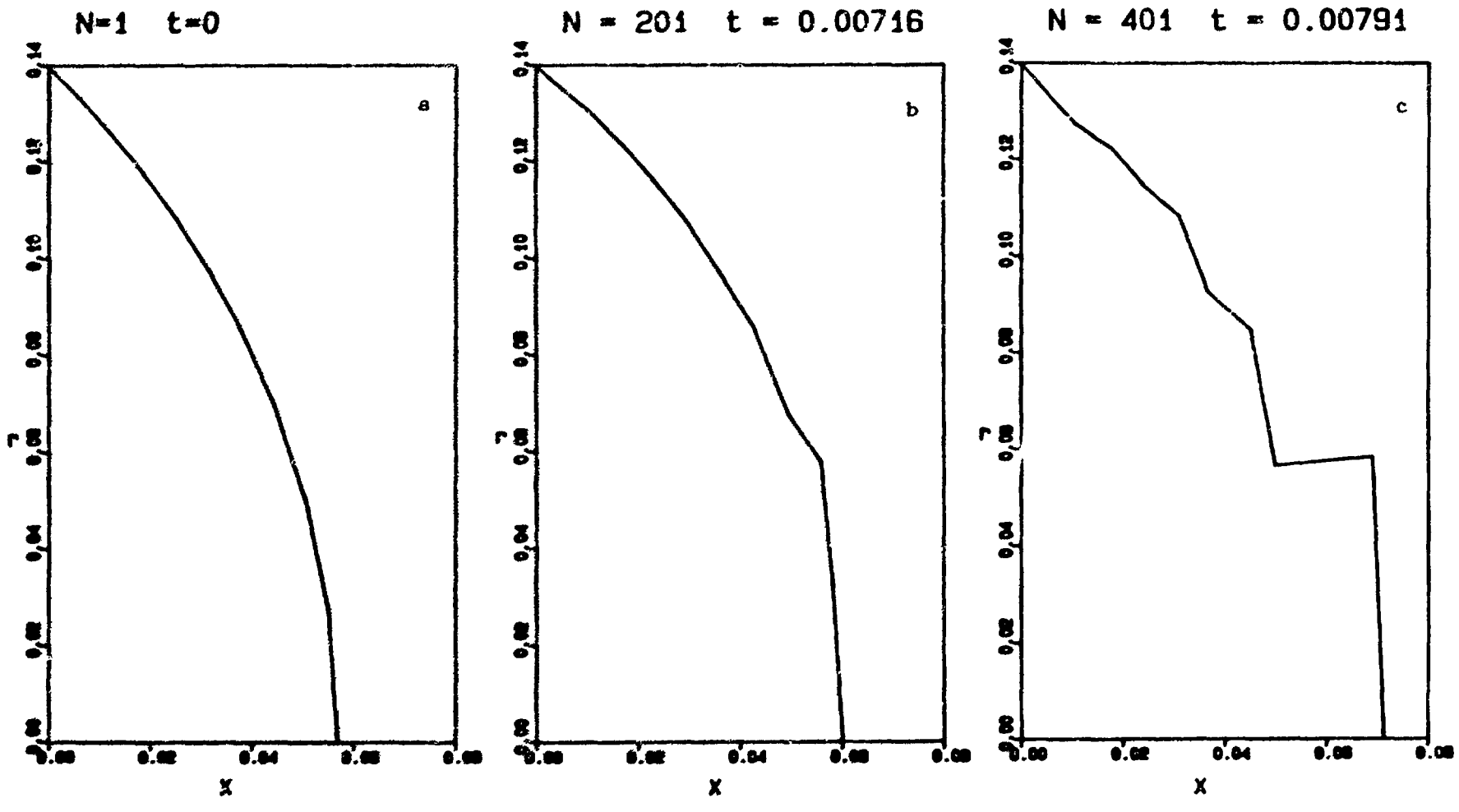

Figure 4.3. Example of unstable transient numerical predictions of droplet formation, 1/16 inch diameter steel, 200 inch/min (plotted in non-dimensional coordinates).

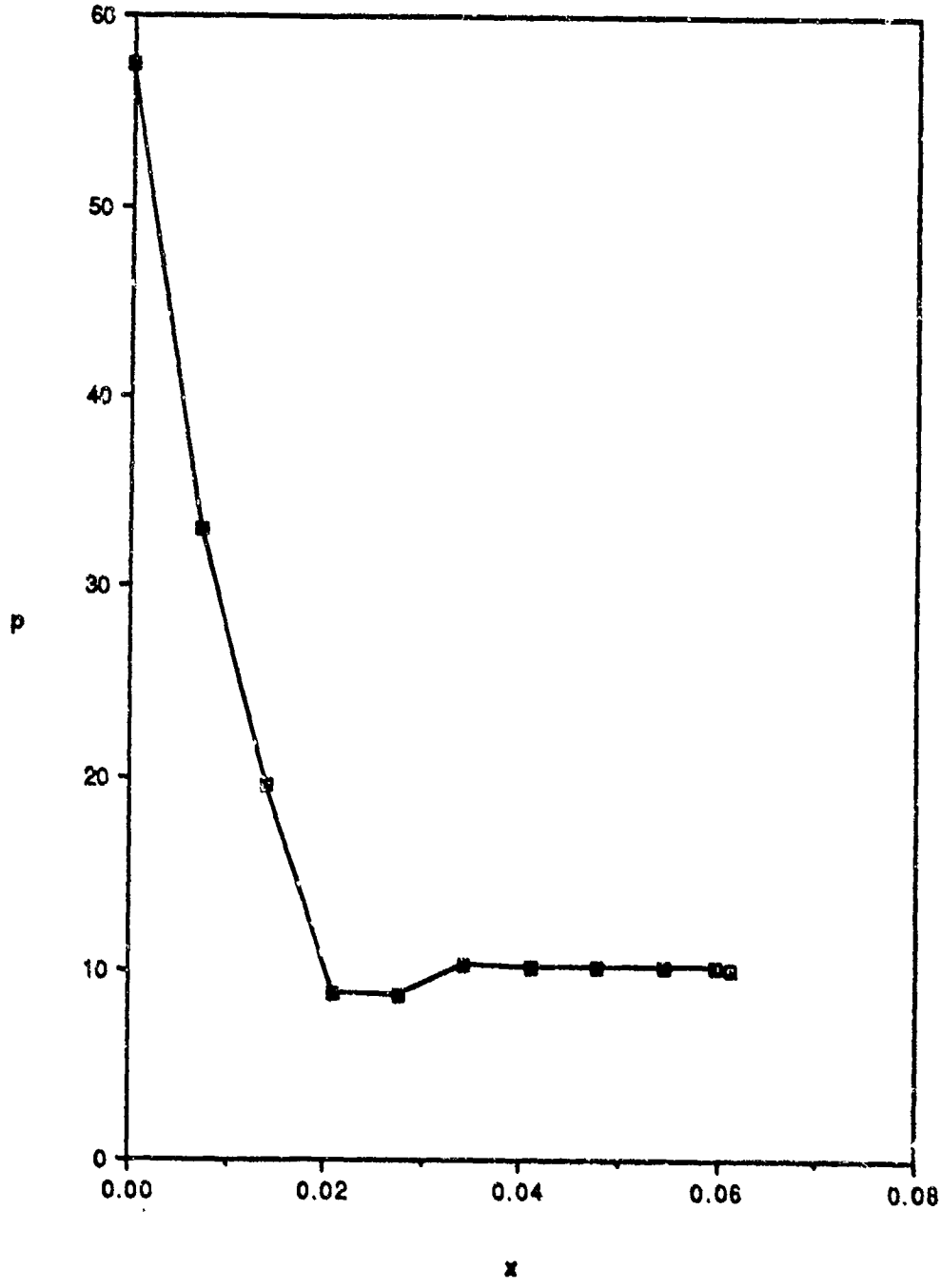

Figure 4.4. Predicted instantaneous pressure profile p(x) during early development, N = 9, $H_{initial}$ = 5.

DMM/ld/0559m

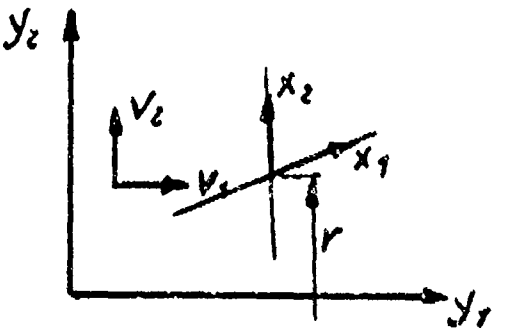

Figure 4.5. Co-ordinate systems and velocity decomposition

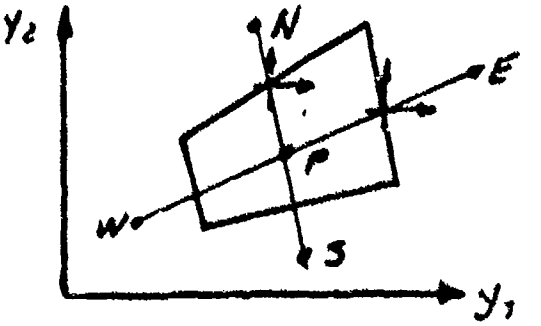

Figure 4.6. Finite volume representation

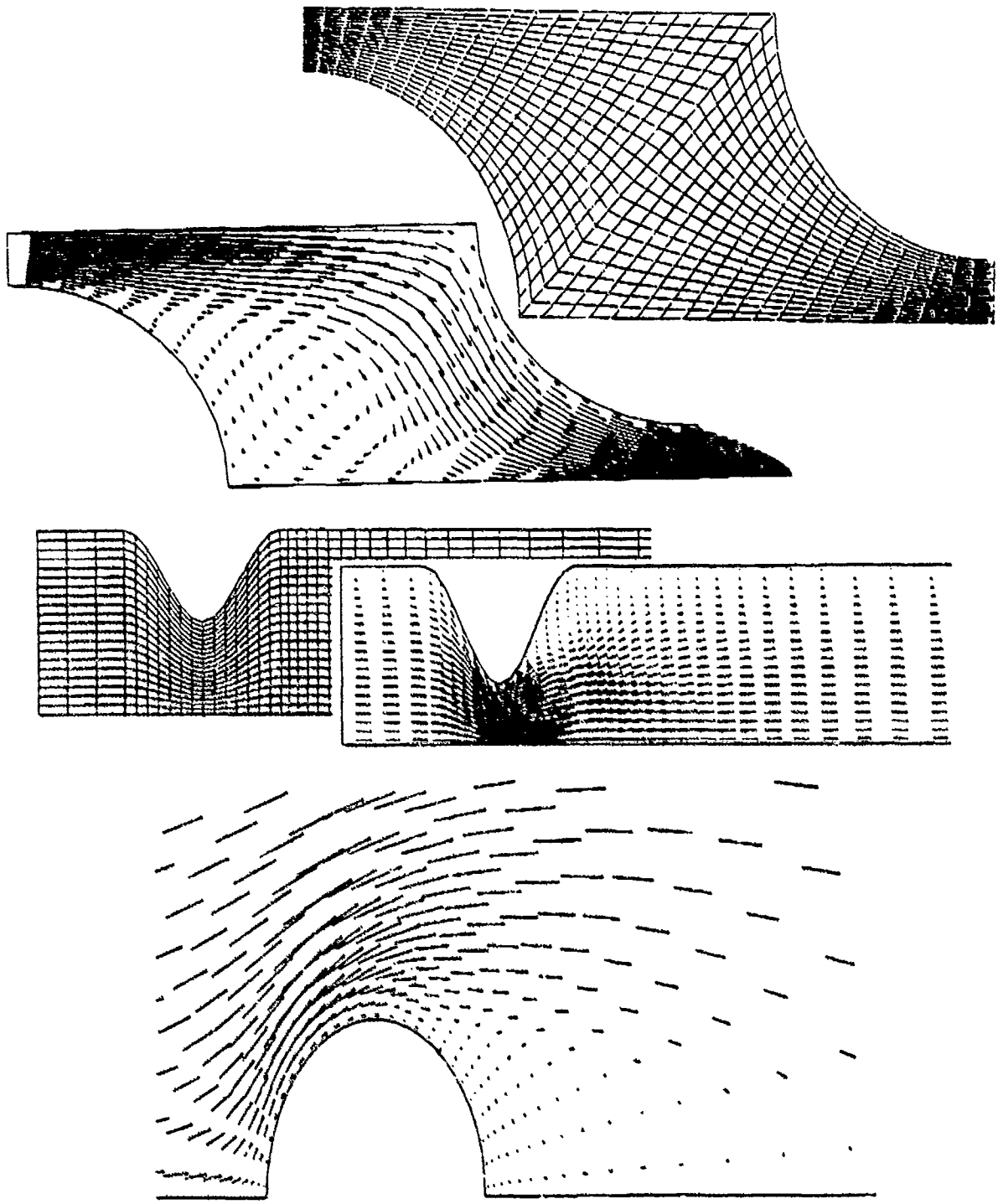

Figure 4.7. Separated flows computed via a non-orthogonal finite-volume algorithm. [Lien and Leschziner, 1989].

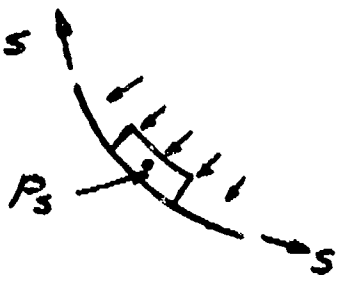

Figure 4.8. Near-surface volume

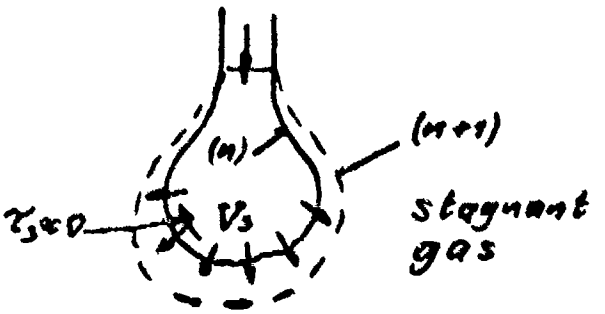

Figure 4.9. Surface adjustment

Appendix A. ANALYSES OF ELECTRODE HEAT TRANSFER IN GAS METAL ARC WELDING

by

Y.-S. Kim,[1,2] T.W. Eagar[1] and D.M. McEligot[3]

Abstract

Thermal processes occurring in electrodes in Gas Metal Arc Welding are considered approximately, experimentally, analytically and numerically for ranges of electrodes and materials of practical importance. Estimation of the governing non-dimensional parameters and pertinent time scales provides insight into the complicated phenomena involved in periodic droplet formation and detachment while demonstrating that the behavior of the solid electrode may be considered to be quasi-steady. Experimental observations of the formation of a tapering tip, forming as electrical current is increased in steel electrodes shielded by argon gas, are found quantitatively consistent with numerical simulations based on the hypothesis that additional thermal energy is evolved along the cylindrical side surface of the electrode due to socalled electron condensation.

1. Materials Science and Engineering, Massachusetts Institute of Technology, Cambridge, MA 02139

2. Now Postdoctoral Research Associate, Materials Science and Engineering, University of Florida, Gainesville, FL 32611

3. Westinghouse Naval Systems Division, Middletown, RI 02840. Professor Emeritus, University of Arizona, Tucson, AZ 85721

ANALYSES OF ELECTRODE HEAT TRANSFER IN GAS METAL ARC WELDING

Y.-S. Kim, T.W. Eagar and D.M. McEligot

1. INTRODUCTION

Gas Metal Arc (GMA) welding is the most common method for arc welding steels, super-alloys and aluminum. About forty percent of the production welding in this country is accomplished by this process in which the thermal phenomena and melting of the solid electrode are coupled to the plasma arc and the weld pool. Thus, the thermalfluid behavior of the electrode and detaching drops can have significant effects on the subsequent weld quality and production rate.

While a number of qualitative hypotheses concerning metal transfer have been suggested and in some instances accepted, quantitative proof of their validity is still lacking [Eagar, 1989]. The purpose of the present paper is to provide quantitative analyses, concentrating on the thermal behavior of the electrode, to aid fundamental understanding of the process. Main emphasis is on the commercially important application of spray transfer [Lesnewich, 1958] from steel electrodes with argon shielding.

For a general review of recent work on metal transfer, the reader is referred to Lancaster's chapter in the text by Study Group 212 of the International Institute of Welding [Lancaster, 1984]. The pioneering study of metal transfer by Lesnewich [1958a, b] has been recently summarized by him in a letter [Lesnewich, 1987]. Cooksey and Miller [1962] described six

modes and Needham and Carter [1965] defined the ranges of metal transfer. Weld quality depends on the mode occurring. The axial spray transfer mode is preferred for gas-shielded metal-arc welding to insure maximum arc stability and minimum spatter.

Analyses and experiments have been conducted by Greene [1960], Halmoy [1980], Woods [1980], Ueguri, Hara and Komura [1985], Allum [1985] and by Waszink and coworkers [1982, 1983, 1985, 1986]. These studies have predominantly addressed steady or static conditions, although Lancaster and Allum did consider transient instabilities for possible explanations of the final stage of the droplet detachment process.

Possible thermal processes which may interact with the forces on the droplet to cause detachment are described schematically in Figure 1.1 for an idealized droplet. The process is transient, possibly periodic, proceeding from detachment of one droplet through melting, formation and detachment of the next, so there is a change in the thermal energy storage $\dot{S}$. Heating is caused by electrical resistance heating (or possibly induction) G and by interaction with the plasma q_p. Heat losses occur via conduction in the solid rod q_k, radiation exchange with the environment q_r, convection to the shielding gas q_c and possible evaporation at the surface q_v. Internal circulation q_{nc} may be induced by electromagnetic, surface tension, gravity and/or shear forces.

The governing thermal energy equation for the wire and droplet can be written in cylindrical coordinates as [Kays, 1966]

$$\frac{\partial \rho I}{\partial t} + \rho u \frac{\partial H}{\partial x} + \rho v \frac{\partial H}{\partial r} = \frac{\partial}{\partial x}\left(k\frac{\partial T}{\partial x}\right) + \frac{1}{r}\frac{\partial}{\partial r}\left(kr\frac{\partial T}{\partial r}\right) + q'''_G \qquad (1.1)$$

where the dependent variables are the enthalpy (H) and the specific internal thermal energy (I). For steady motion of the solid wire, the radial velocity (v) disappears and the axial velocity (u) is uniform at the wire feed speed V_w. The volumetric thermal energy generation rate (q_G''') is a consequence of resistive (or Joulean) heating. If the boundary conditions and other quantities can also be idealized as steady in time, then the first term (representing transient thermal energy storage) also disappears.

For the droplet these idealizations are not valid. The velocity field must be determined from solution of the continuity and momentum equations after solving Maxwell's electromagnetic field equations to obtain body force terms. The droplet grows so the process is non-steady and the transient terms must be retained (as they might be for the solid wire since the melting interface also must be affected by the transient droplet). Boundary conditions for the momentum equations include treatment of the surface tension forces which can be dominant. Solution for the droplet fields is thus much more difficult than analysis of the thermal behavior of the solid wire and is beyond the scope of the present work.

The present study examines the thermal processes occurring in moving electrodes for GMAW with the objectives of (1) determining which phenomena are important in controlling the melting rate and (2) explaining the formation of a tapering tip observed for some combinations of electrode materials and shielding gases.

In section 2 the governing parameters are identified and related thermal-fluid time scales are estimated. Pertinent experimental observations by Kim

[1989] are presented next, followed by closed form analyses for thermal conduction in the moving solid electrode under the idealization of constant material properties. To account for significant variation of the electrical resistivity with temperature, an available numerical method is applied; section 5 describes the technique while section 6 presents simulations related to the conditions of the experiments of section 2. We conclude with a summary of the major observations deduced.

2. NON-DIMENSIONAL PARAMETERS AND TIME SCALES

To quantify the typical orders-of-magnitude included, the approximate properties and welding parameters for steel are employed. In applications for steel, typical wire diameters are in the range 0.8 to 2 mm (0.03 to 0.09 in.) and wire speeds are of the order 0.04 to 0.2 m/sec (100 to 400 in./min). The wire extension beyond the electrical contact tip is about 10 to 30 mm (1/2 to 1 in.) [Eagar, 1987]. Typical thermofluid properties of steel (or iron) in solid and liquid phases have been given by Greene [1960] and Waszink and Piena [1985] and others.

The Reynolds number of the droplet, $Re = \rho V d/\mu$ based on wire diameter and feed rate and liquid metal viscosity, is of the order of 100 for steel. Even if a no-slip condition were applied at the surface as in duct flow, one would expect the flow in the droplet to be laminar. But, since the liquid surface is not constrained, the shear stresses are expected to be much less, so there is more reason to believe the circulation within the droplet to be laminar, perhaps even so-called creep flow.

The Prandtl number of the liquid metal, $Pr = c_p \mu/k$, is a measure of the

rate at which viscous effects propagate across the fluid relative to thermal conduction [Kays, 1966], or the rate at which the flow field approaches steady state compared to the temperature field. For steel and most liquid metals $Pr \lesssim 0.1$, so the thermal field adjusts to the flow field much quicker than the flow adjusts to its disturbances.

The importance of axial thermal conduction upstream in a fluid (or the solid wire) relative to the motion can be estimated via the Peclet number,

$$Pe = \frac{Vd}{\alpha} = \frac{\rho V c_p d}{k} = \frac{\rho V d}{\mu} \frac{c_p \mu}{k} = Re \cdot Pr \qquad (1.2)$$

For $Pe \gtrsim 200$, the axial conduction term may be neglected relative to the other terms in the energy equation (1.1) [Kays, 1966]. On the other hand, a low Peclet number corresponds to the situation where thermal conduction is much more effective at transporting thermal energy axially than motion of the medium, as will be seen later in Section 4.

A criterion for the appearance of approximately isothermal conditions is given by the Biot number, $Bi = h \cdot Vol/(k_{solid} \cdot A_s)$, where h is a heat loss coefficient for convection and/or radiation. For the temperature distribution radially across a cylindrical section, it becomes $Bi = h \cdot d/(4k_{solid})$. If $Bi \ll 1$, the temperature variation across the medium is much less than the difference between the surface and surroundings, i.e., isothermal. Conversely, a large Biot number implies that thermal conduction resistance in the medium dominates the problem establishing the temperature distribution.

Thermocapillary, or "Marangoni", convection has been shown by a number of

investigators [Heiple and Roper, 1982; Oreper, Eagar and Szekely, 1983; etc.] to have significant effects on the thermofluidmechanics of weld pools. For droplet formation, its effects do not appear to have been considered in detail. Surface tension generally depends on temperature, composition and electrical potential. Lai, Ostrach and Kamotani [1985] have examined the role of free-surface deformation in unsteady thermocapillary flow; while their geometries differ from liquid droplets, their results should provide order-of-magnitude estimates for the present problem. Further, for short times when the motion is still confined to a thin region near the surface, the results for the dissimilar geometries should approach each other; i.e., both cases should be effectively one-dimensional, transient, semi-infinite situations.

The importance of steady thermocapillary convection can be estimated from a number of non-dimensional parameters:

1) "Static bond number"

$$Bd = \frac{\rho g D^2}{\sigma}$$

hydrostatic effects relative to surface curvature effects on pressure

2) "Elevation Bond number"

$$Bo = \frac{\rho g D^2}{|\partial\sigma/\partial T|\Delta T}$$

$$\frac{\text{hydrostatic pressure}}{\text{thermocapillary dynamic pressure}}$$

3) "Dynamic Bond number"

$$Bo_d = \frac{\rho g D^2 \beta}{|\partial\sigma/\partial T|}$$

$$\frac{\text{natural convection}}{\text{thermocapillary convection}}$$

The direction of flow due to thermocapillary convection depends on whether the surface tension increases or decreases with temperature. In a sense, a

region with higher σ pulls fluid from regions with lower σ. For very pure steels $\partial\sigma/\partial T$ is negative so the flow tendency would be from warmer to cooler. In the vertical geometry considered here, that would be from the warm liquid drop towards the melting zone and might inhibit detachment. With small amounts of contaminants, such as sulfur or oxygen as in the weld pool studies of Heiple and Roper [1982], $\partial\sigma/\partial T$ can become positive so the tendency would be towards enhancing detachment forces. In either case the thermal field near the melting interface would be modified to some extent.

To estimate values of the thermocapillary parameters for a liquid steel droplet, we take the temperature range as being from the melting point to a maximum about 500K below the boiling point [Block-Bolten and Eagar, 1984]. Following Waszink and Graat [1983], we took surface tension values for mild steel to be dominated by the manganese constituent with $\sigma \approx 0.9$ N/m (0.005 lbf/in) and $|\partial\sigma/\partial T| \approx 0.2 \times 10^{-3}$ N/mK (6×10^{-7} lbf/in F).

Estimated orders-of-magnitude and ranges of these thermal parameters become

	Re	Pe	Bi	Bd	Bo	Bo_d
Globular	50	4	0.001	2	10	0.8
Spray	500	40	0.001	0.2	1	0.08

Here the Biot number refers to radial heat transfer (rather than axial transfer from the liquid droplet to the melting interface). The values of the Peclet number imply that wire motion is more significant but that axial thermal conduction is not entirely negligible.

With the exception of Bo for globular transfer and Bo_d for spray transfer, the thermocapillary parameters are all of order one. For globular

transfer hydrostatic pressure would be expected to be significantly greater than the thermocapillary dynamic pressure. And for spray-sized droplets, Marangoni convection would be significantly greater than natural convection. The value of $Bd \approx 0.2$ for spray transfer would be an indication that a force(s) other than gravity is involved in droplet detachment in that mode, since surface curvature would cause greater pressure (and restoring force) than the weight of the drop. Greene [1960] and Waszink and Piena [1985] have concluded from different arguments that the additional forces are electromagnetic and, therefore, Maxwell's equations should be included in the complete solution.

The discussion of the non-dimensional governing parameters above applies primarily to steady processes. However, droplet formation and detachment is a non-steady event so time scales or response times of the phenomena must also be considered to estimate whether steady or quasi-steady conditions may be approached during the process [McEligot and Uhlman, 1988].

For 1.6 mm (1/16 in.) diameter mild steel, Lesnewich [1958b] shows droplet detachment frequencies to be of the order of 15 per second for currents below 240 amp and 250-300 per second above 280 amp. These values represent globular and spray metal transfer and correspond to periods of about 70 ms and 3 ms, respectively. For his experiments with 1.1 mm (0.045 in.) diameter steel, Morris [1989] reports typical values of 50 ms for globular and 4 ms for spray transfer but has seen up to 2000 drops/sec or droplet periods as short as 1/2 ms.

The time for a thermal change to approach steady state (within about

five per cent) by conduction in the radial direction [Kreith, 1973], the thermal conductive time scale, can be estimated as $\theta_T \simeq 0.6\ r_o^2/\alpha$.

The viscous time scale to approach steady state can be expected to be analogous to the thermal conductive time scale, or $\theta_v \simeq 0.6\ r_o^2/\nu = 0.6\ \theta_T/Pr$. (Allum [1985 a] quotes Sozou and Pickering [1975] as saying that for J x B flows to approach steady state requires $\theta \sim L^2/\nu$, i.e., another viscous time scale.) Temperature variation near the surface affects the surface tension and, therefore, the droplet shape particularly near the neck at detachment. Consequently, one must consider times to modify the surface layers rather than only the approach to steady state. For radial conduction in a cylinder, a 90% change in temperature is predicted at $r/r_o = 0.9$ within non-dimensional time $(\alpha\ \theta/r_o^2) \simeq 0.1$, approximately. This time scale is about 1/6 of that for full thermal penetration.

For their weld pool simulation Kou and Wang [1986] claim the characteristic times associated with electrical conduction are of the order of 10^{-12} sec. Since these time scales probably have an r^2 dependence and the weld pool covers a larger region than the droplet, the corresponding times can be expected to be less than 10^{-8} ms in the present problem. Typical power supplies show a "ripple" of about five percent in the electric current (unless they are stabilized) at 60, 120 or 360 Hz. This situation implies about a 10% variation in i^2 with a period of 16, 8 or 3 ms, respectively. Thus, this process is usually slow relative to spray detachment and fast relative to globular detachment, but in either case it could be expected to affect a periodic detachment process upon which it is superposed.

A time scale for the propagation of capillary waves can be formed from the

fluid properties as $\Theta_c = [8\sigma/(\rho g^3)]^{1/4}$. For steel it is of the order 30 ms. The natural frequency of the fundamental mode for surface oscillation of a sphere of liquid surrounded by an infinite region of gas [Lamb, 1932, Sec. 275; Clift, Grace and Weber, 1978] can be approximated as $f^2 = 16\sigma/(\pi^2 \rho d^3)$. A time scale to correspond to a significant surface oscillation might be taken as 30/360 of the period of oscillation.

A variety of thermocapillary time scales can be deduced for this problem [McEligot and Uhlman, 1988]. Pimputkar and Ostrach [1980] analyzed transient thermocapillary flow ("Marangoni convection") in thin liquid layers. They found the appropriate time scale for small times to be $\Theta_M = h^2/\nu$ (where h is the height of the layer), i.e., yet another viscous time scale. The thermal time scale was $\Theta_{MT} = h^2\ Pr/\nu$. The large time solution has a scale $\Theta_{ML} = L/U$ where L is a measure of the streamwise length and the characteristic velocity of the thermocapillary driving force is $U = |\partial\sigma/\partial T|\Delta(T - T)/\mu$. For their problem there was a significant velocity change before $\Theta \approx 0.1\Theta_M$ and a steady Couette flow was approximately reached by $\Theta \approx \Theta_M$; significant surface distortion was predicted for $\Theta >$ 0.01 L/U or less. Other appropriate thermocapillary time scales may be estimated from (1) the time necessary for the induced surface velocity to become comparable to the wire velocity, (2) the residence time for a fluid particle to traverse half the circumference due to the axial temperature gradient,

$$\Delta\Theta \simeq \frac{\pi d}{2U} \simeq \frac{\pi^2}{16} \frac{\rho_\ell c_p \mu V_w d^4}{|\partial\sigma/\partial T| i^2 \rho_e}$$

and (3) the predicted residence time corresponding to the flow induced during a typical droplet period using the analysis of Lai, Ostrach and Kamotani [1985, Fig. 4]. These four different approaches give a range greater than an order-of-magnitude for the potential thermocapillary time scales.

DMM/ld/0559m

The results of the time scale estimation for 1.6 mm (1/16 in.) diameter steel are presented in Table 2.1. It must be emphasized that these are merely order-of-magnitude estimates for guidance. In general, when the response for one phenomenon is much quicker than another, the first can be treated as quasi-steady relative to the second. When time scales are of the same order, both phenomena must be considered in the transient analysis. From the comparison, we see that viscous diffusion is too slow to be important except as involved in the thermocapillary surface phenomena. The proper time scale for thermocapillary convection in this application has not been determined; due to the range of values estimated, one can only say it may be important for globular and/or spray transfer. For globular and spray modes thermal conduction at the surface and surface oscillations have time scales comparable to their periods. Interaction with electric current oscillations depends on the power supply frequency (and whether it is stabilized effectively).

In summary, for the general case of electrode melting and detachment the order-of-magnitude estimates of governing parameters and time scales reveal no significant simplification except that buoyancy forces are likely to be negligible in the droplet. Ultimately, it will probably be necessary to solve the transient, coupled thermofluidmechanic equations for the droplet and wire in conjunction with experimental observations to obtain predictions with reasonable detail. The present study begins that process, concentrating on the solid electrode.

3. MELTING EXPERIMENTS

Measurements were obtained with research welding equipment to observe the electrode shape, arc attachment, droplet size, transfer modes and their rela-

tionships to typical welding control parameters. These experiments established the conditions for which numerical simulations were later conducted.

3.1 Apparatus

Welding was by the Direct Current, Electrode Positive or "reversed polarity" technique. The welding equipment used in this study included two Miller "Gold Star" power supplies, a Linde UEC-8 weld controller, a Linde SHE-11 'low inertia' wire feed motor and a Linde ST-12 GMAW Torch. The two Miller power supplies were operated in parallel and could provide a total output current of over 1200 amperes. The UEC-8 controller was operated in constant current mode to match the transistorized current regulator which will be described later. The Linde SHE-11 'low inertia' wire feed motor was used since constant current and pulsed current welding were being used. The Linde ST-12 torch was modified to ensure a relatively constant contact point between the contact tip and the consumable electrode; an alumina tube was inserted into the contact tip leaving only 5 mm for electrical contact rather than the nominal contact length of 24 mm.

In addition to this commercially available equipment, some laboratory-built equipment was used as a part of the welding system. These included a transversing table and the welding power regulator. The weld table moved the weld specimen so that the weld torch could remain at a fixed position. The table is powered by a DC motor and provides constant weld speed up to five cm/sec.

The welding power regulator used in this study was of the constant current type and can supply DC current with less than 1% ripple. The regulator is a

transistorized current controller which was designed by Alexander Kusko, Inc. of Needham, Massachusetts, and was constructed in the MIT Welding Laboratory [Eickhoff, 1988]. This system uses transistors to control the welding current and is capable of pulsing the DC current to a maximum of 5 kHz for small superimposed signals. This equipment is extremely flexible in providing pulsing conditions; peak current, base current, peak time and base time can be controlled independently from a Tektronix FG501A function generator included with the controller.

Analysis of the metal transfer process was performed using high speed videophotography. In contrast to the conventional high speed cinematography which uses a light source with greater intensity than the arc and a strong neutral density filter, in this study a laser backlighted shadowgraphic method [Allemand et al., 1985] was used. This system excludes most of the intense arc light and transmits most of the laser light by placing a spatial filter at the focal point of the objective lense. The system setup and the equipment specifications are detailed by Kim [1989].

The high speed video system consists of an Ektapro 1000 motion analyzer from Eastman Kodak Co., and is capable of producing images at a maximum 1000 full frame pictures per second (pps) and at a maximum of 6000 pps with split frames. After the picture is recorded at high speed on high density tape, the images can be transferred to a normal VHS recorder for analysis.

3.2 Procedures and ranges of variables

Measurements emphasized mild steel (AWS E70s-3) as the electrode material but aluminum alloys (AA1100 and AA5356) and titanium alloy (Ti-6Al-4V) were

also employed to include a wider range of physical properties. An electrode diameter of 1/16 in (1.6 mm) was used throughout. The shielding gases employed were pure argon, pure helium, their mixtures, argon-2% oxygen and carbon dioxide. The ranges of variation of welding parameters during this study are given in Table 3.1; overall welding current ranged from 80 to 420 amp and electrode extension was set at 16, 26 or 36 mm.

After installing the electrode wire in the torch, measurement conditions were adjusted as follows. The Linde UEC-8 weld controller was operated in the constant current mode. The desired electrical current and weld table speed were first set. During a preliminary run the electrode extension was set by observing the distance via the video camera with laser back light illumination while adjusting the open circuit voltage. The values obtained were then employed for fresh welds during the actual measurements.

Electrode extension is defined in this study as the distance from the end of the contact tip to the liquid-solid interface. With the video monitoring technique it could be controlled within $\pm$ 1 mm during welding. Electrical current was measured by an external shunt which is capable of measurement within an uncertainty of $\pm$ 1% of full scale.

Melting rates were measured by reading the output voltage of a tachometer which was in contact with the moving electrode. The output voltages of the tachometer and of the current shunt were recorded with a Honeywell 1858 'Visicorder Oscillograph' in conjunction with a low band pass filter.

The tachometer was carefully calibrated by indenting the surface of the electrode once every second with a solenoid indenter triggered by a rotating

cam. Afterwards the indented sections of the electrode were removed and the actual mass of the electrode passing through the system per unit time was measured. The mass of the electrode was weighed with a balance which has accuracy of 0.0005 g. The calibration was performed by measuring the mass which passed through the indentor for five seconds.

3.3 Experimental results

Typical data for melting rates (or wire feed speeds V_w) with steel and a range of shielding gases are presented in Figure 3.1. The same trends were seen at shorter and longer extensions [Kim, 1989]. With argon, as well as with A-2%O_2, there is an apparent slight variation in the trend of the curve, or a "transition", at intermediate currents. With helium and carbon dioxide as shielding gases this effect was not evident; the slopes of the curves were continuous and near constant.

For mixtures with an argon rich composition (75% A/25% He) there also is an apparent transition in the melting rate curve. However, as the helium content is increased (50% A/50% He), it disappears as with helium and carbon dioxide. Aluminum and titanium revealed slight transitions in their curves when shielded with pure argon. Thus it seems that the transition is related to the behavior with argon gas.

For the same variety of welding conditions, droplet sizes were determined. The size was measured from the still image on the video screen once every ten seconds, then these ten samples were averaged. Figure 3.2 compares the results for steel with A-2%O_2, helium and CO_2 as the shielding gases. Again there is a substantial difference in behavior depending on shielding gas, but no

critical transition in size is observed. Calculations of the related droplet detachment frequencies also failed to show any sharp transition. However, with argon much smaller droplets are evident at high currents.

Visualization of the electrode and droplet detachment provides some insight into the effects of argon on the metal transfer process. Figure 3.3 demonstrates the effect of electrical current on the size of the detached droplets and the shape of the solid electrode for steel and argon over the same range as Figures 3.1 and 3.2. A continuous, gradual variation is seen. If one defines the transition to spray transfer as occuring when the droplet diameter is approximately equal to the wire diameter, it is seen in the middle subfigure for i ≈ 253 amp; this value agrees with the observations of Figure 3.2.

At low currents the photographs show large subglobular droplets and a relatively blunt tip to the electrode. As the current is increased, (1) the droplets become smaller, (2) the required wire speed increases and (3) the electrode tip acquires a sharpening taper. The sequence is continuous and gradual.

No taper was observed with shielding by helium or CO_2; instead visualization showed a repelled form of detachment which led to large drop sizes. With aluminum and argon shielding, a taper formed but was shorter (or blunter) than for steel. None was seen for DC operation of titanium electrodes to 260 amperes (maximum used), but it did occur with pulsed currents at 500 amperes so it is expected for higher DC currents with argon.

Consideration of the electron current path yields further understanding. The distribution of current on the surface of the electrode is affected by several factors, such as material, shielding gas and total welding current.

Precise measurement of the distribution is not available. However, in Kim's study [1989] an approximate method, considering the main current path to be related to the bright spots on the photographs, gave useful indications. These observations of anode spot behavior were made with a color video camera using the laser back-light system. Instead of the narrow band filter used with the high speed video, a neutral density filter was used to adjust the light input to the camera.

Figure 3.4 shows observed bright spots or indicated current paths for steel and titanium alloy in globular transfer and steel in streaming transfer, all with argon. In steel there is no well-defined current path into the consumable electrode. Rather, the arc root appears to be diffuse. Therefore, it seems that the electrons condense not only on the liquid drop but also on the solid side surface of the electrode. Comparable phenomena were observed with aluminum. With the titanium alloy there is a sharp anode spot on the liquid drop, with a strong plasma jet emanating from this spot, and most of the electrons seem to condense on the liquid drop at this spot.

With CO_2 shielding, most of the electrons condense at the bottom of the liquid drop. With helium, the electron condensation is confined to the lower bottom but is less concentrated than with CO_2 [Kim, 1989].

As a consequence of the above observations, the following hypothesis of taper formation is proposed [Kim, 1989]: When the shielding gas is argon, a portion of the electrons condense on the cylindrical side surface of the solid electrode and liberate heat of condensation at this location. When this energy generation rate is high enough on the surface, the electrode surface will melt and the liquid metal film will be swept downward by gravitational and/or other

forces. When this melting occurs over a sufficient length of the cylinder, a taper will develcp at the end of the electrode. Whether this hypothesis is quantitatively consistent with the thermal phenomena in the solid electrode is a question which is examined analytically in the later sections.

4. PRELIMINARY ANALYSES FOR SOLID ELECTRODE

As an introduction to the next section, and to provide further insight, this section provides discussion of two limiting closed form analyses: (1) resistive heating of the electrode without heat transfer through the side surface and (2) heating at the side surface without axial conduction. In both cases material properties are treated as constant and the fields are approximated as steady.

The steady idealization implies that the dimensions of interest are large relative to the penetration depth for thermal conduction at the droplet detachment frequencies and/or that the predictions represent effective temporal averages. This penetration depth can be estimated from the transient conduction solution for a cosinusoidally oscillating surface temperature on a semi-infinite solid [Boelter et al., 1965, eqn 6.12a]. For the n-th harmonic about the mean it takes the form

$$T - T_{mean} = T_o \exp\left\{-\left(\frac{n\pi}{\alpha P}\right)^{1/2} x\right\} \cos\left\{\frac{2\pi n}{P} t - \left(\frac{n\pi}{\alpha P}\right)^{1/2} x\right\} \qquad (4.1)$$

The depth at which the amplitude is a fraction $1/\nu$ of the surface amplitude is then

$$\Delta x = (\ell n\ \nu) \cdot \sqrt{\alpha P/(n\pi)} \qquad (4.2)$$

From the first harmonic and a five percent criterion, one may estimate this

penetration depth to be about $0.1d_w$ for spray transfer and $0.6d_w$ for globular transfer for steel in the present experiments. There may be a bit more variation due to the actual size of the drops but it would be countered by the convective wire motion in the opposite direction to the thermal disturbance.

4.1 One-dimensional thermal conduction

The one-dimensional idealization corresponds to conditions where all the heating by electron condensation occurs at the tip and there is no significant heat loss (or gain) at the cylindrical surface of the electrode. In this situation, the governing energy equation (1.1) may be reduced and non-dimensionalized to the form

$$\frac{d^2\bar{T}}{d\bar{z}^2} + \frac{d\bar{T}}{d\bar{z}} = \bar{q}_G \tag{4.3}$$

where $z = L - x$ is measured from the molten tip so $u = -V_w$ and the non-dimensional variables are

$$\bar{T} = (T_m - T)/(T_m - T_r)$$

$$\bar{z} = (V_w z/\alpha) = zPe/D$$

and

$$\bar{q}_G = \frac{q_G''' D^2}{k(T_m - T_r)Pe^2} = \frac{16}{\pi^2} \frac{i^2 \rho_e}{kD^2(T_m - T_r)Pe^2} \tag{4.4}$$

Appropriate boundary conditions are

$$\bar{T} = 0 \text{ at } \bar{z} = 0$$
$$\bar{T} = 1 \text{ at } \bar{z} = \bar{L} = LPe/D \tag{4.5}$$

The solution of this mathematical problem with $\bar{q}_G$ taken constant may be written

$$\bar{T}(\bar{z}) = (1 - \bar{q}_G\bar{L})\left[\frac{1 - e^{-\bar{z}}}{1 - e^{-\bar{L}}}\right] + \bar{q}_G \cdot \bar{z} \tag{4.6}$$

where the first term represents contribution of the thermal conduction from the molten interface, transported upstream against the motion, and the second is the consequence of resistive heating by the electrical current. In section 2 we saw that for steel electrodes we can expect $4 \lesssim Pe \lesssim 40$ and in the experiments L/D was about 10 to 20 so the denominator is near unity, giving the approximation

$$\bar{T}(\bar{z}) \simeq (1 - \bar{q}_G \bar{L})\left[1 - \exp\left|-\bar{z}\right|\right] + \bar{q}_G \bar{z}$$

or

$$\frac{T - T_m}{T_m - T_r} \approx - (1 - \bar{q}_G \bar{L})\left[1 - \exp\left|-\bar{z}\right|\right] - \bar{q}_G \bar{z} \qquad (4.7)$$

which decreases from zero to -1 (i.e., T(z) from T_m to T_r) as $\bar{z}$ increases away from the tip.

The exponential term (or a plot of the solution) shows that the effect of thermal conduction from the melting interface becomes negligible beyond $\bar{z} \gtrsim 5$ or $z/D \gtrsim 5/Pe$. For even the lowest Peclet number expected, this is only of the order of one diameter upstream. As V_w (and therefore Pe) increases, the distance becomes less yet.

The fraction of the total temperature rise from T_r to T_m due to conduction from the interface is approximated by the term $(1 - \bar{q}_G \bar{L})$. The non-dimensional quantity $\bar{q}_G$ may be seen to be the asymptotic slope of the curve $\bar{T}(\bar{z})$ away from the molten tip; for $i \simeq 200$ amp at 1000K with 1.6 mm steel, typical values would be of the order $\bar{q}_G \simeq 0.5/Pe^2$. However, it must be re-emphasized that these results can only considered to be qualitative. The quantity $\bar{q}_G(\bar{x})$ varies substantially since ρ_e increases by a factor of about eight for steel between T_r and T_m so the slope of the contribution by resistive heating will also increase as T_m is approached.

DHM/ld/0559m

4.2 "Electrode convection"

With axial thermal conduction neglected, the governing energy equation (1.1) can be written for symmetrical conditions as

$$\frac{\partial T^+}{\partial x^+} = \frac{1}{r^+}\frac{\partial}{\partial r^+}\left(r^+\frac{\partial T^+}{\partial r^+}\right) + q_G^+ \qquad (4.8)$$

with $x = 0$ at the entry corresponding to the contact tip and increasing in the direction of motion. The non-dimensional variables are defined as

$$T^+ = (T - T_{in})/T^* \quad , \quad q_G^+ = q_G''' r_s^2/(kT^*)$$

+ $$x^+ = (2x/r_s)/Pe \quad \text{and} \quad r_s = (r/r_s)$$

where the definition of reference temperature T^* would be chosen by convenience, depending on the surface boundary condition. From symmetry, the centerline boundary condition would be $(\partial T^+/\partial r^+) = 0$ at $r^+ = 0$. And the initial condition is $T^+ = 0$ at $x^+ = 0$.

Equation (4.8) may be seen to have the same form as for transient conduction in an infinitely long circular rod with a heat source (e.g., equation 3.15 of Boelter et al. with their diffusivity a = 1). Typically it may be solved by separation of variables and superposition chosen depending on the surface boundary condition. As shown by Boelter et al., the temperature field can be separated into two components, $T^+ = T_1 + T_2$ where

$$T_1 \text{ satisfies } \frac{\partial T_1}{\partial x^+} = \frac{1}{r^+}\frac{\partial}{\partial r^+}\left(r^+\frac{\partial T_1}{\partial r^+}\right)$$

and

$$T_2 \text{ satisfies } \frac{1}{r^+}\frac{\partial}{\partial r^+}\left(r^+\frac{\partial T_2}{\partial r^+}\right) + q_G^+ = 0$$

General solutions of these equations are

$$T_{1,n} = C_n \left\{ \exp -\gamma_n^2 x^+ \right\} J_o(\gamma_n r^+) \tag{4.9}$$

and

$$T_2 = -\frac{r^{+2}}{4} q_G^+ + C_2 \tag{4.10}$$

where the γ_n are eigenvalues and C_n are their associated constants to be determined from the boundary and initial conditions.

For electron condensation on the side surface of the electrode an appropriate boundary condition would be a specified surface heat flux distribution $q_s''(x)$, giving

$$\left(\frac{\partial T^+}{\partial r^+} \right)_{r^+ = 1} = -\frac{q_s''(x)\, r_s}{kT^*}$$

The usual approach to this problem would be to obtain a solution for a step change to a constant surface heat flux at x = 0 and to employ that solution with Duhamel's superposition technique to evaluate the specified variation. This approach has been demonstrated in the text by Kays [1966] and, in more detail, in a thesis by H.C. Reynolds [1968; Reynolds, Swearingen and McEligot, 1969]. It is considered beyond the scope of the present work, but qualitative simulations may be obtained by examining a related thermal entry problem.

The classical problem of a step change in surface temperature at the inlet [Schneider, 1957] provides a reverse situation compared to the present problem. The radial temperature difference is large at the inlet and then decreases, giving decreasing $q_s''(x)$ as x increases. In contrast, we picture $q_s''(x)$ increasing with x due to the electron condensation near the molten tip. That is, the temperature profiles near the inlet in the classical problem may be pictured (approximately) as occurring in reverse sequence near the end in our problem; this

effect is superposed upon the increase in wire temperature due to resistive heating as in section 4.1. Figure 4.1 presents the qualitative simulation resulting from this line of reasoning and provides a forecast of expectations for more complete numerical predictions accounting for axial conduction, material property variation and hypothesized distributions of the electron condensation.

5. NUMERICAL PREDICTIONS FOR SOLID ELECTRODE

The purpose of the numerical analyses is to provide means of examining whether the hypothesis of arc heating of the sides of the electrode is consistent with the thermal observations of the experiments. Thus, calculations were conducted at conditions corresponding to some of the individual experiments.

The thermal problem was approximated as steady, with time-averaged values from the experiments used for boundary conditions where necessary. For steady motion of the solid electrode, the governing thermal energy equation (1.1) may be reduced and rearranged to

$$\rho V_w \frac{\partial H}{\partial x} = \frac{\partial}{\partial x}\left(\frac{k}{c_p}\frac{\partial H}{\partial x}\right) + \frac{1}{r}\frac{\partial}{\partial r}\left(\frac{kr}{c_p}\frac{\partial H}{\partial r}\right) + q_G''' \qquad (5.1)$$

The resistive heating term can be evaluated as

$$q_G''' = J^2\rho = i^2\rho/(\pi r^2)^2 \qquad (5.2)$$

provided the electrical current density is taken as uniform across the cross section. Preliminary numerical solutions of the (electrical) potential equation demonstrated this assumption to be valid for the purposes of the present work [Kim, 1987].

The temperature dependencies of the steel properties may be expressed as piecewise-continuous polynomials over successive temperature ranges. For example, electrical resistivity may be represented as

$$\rho_e(T) = a_1 + b_1 T + c_1 T^2 \qquad \text{for } T < T_1 \tag{5.3}$$
$$= a_2 + b_2 T + c_2 T^2 \qquad \text{for } T_1 < T < T_2$$

and so forth.

Appropriate steady thermal boundary conditions are:

Uniform inlet temperature, $T = T_r$ at $x = 0$ (5.4)

Gaussian surface heat flux due to electron condensation,

$$q_s'' = \frac{\alpha i V_c}{\pi r_w} \cdot \frac{1}{\sigma\sqrt{2\pi}} \exp\left\{ - \frac{(L - x)^2}{2\sigma^2} \right\} \qquad \text{at } r = r_w \tag{5.5}$$

where $V_c = (3kT/2e) + V_a + \phi$

Uniform interface heat flux at electrode tip,

$$q_i'' = (q_{total} - q_s - q_G)/\pi r_w^2 \qquad \text{at } x = L \tag{5.6}$$

Radiation and convection losses from the heated electrode can be accounted for with q_s or may be neglected. A measure of the length of the wire surface heated by electron condensation is given by the Gaussian distribution parameter, σ, and α is the fraction which occurs on the side surface. The quantities V_a and ϕ represent anode voltage drop and work function, respectively. The total energy transfer rate q_{total} is given by

$$q_{total} = \dot{m}\,\Delta H = \rho V_w\,\pi\,r_w^2\,\Delta H \qquad (5.7)$$

where ΔH is the enthalpy increase above the reference temperature required to melt unit mass of the material.

When there is electron condensation on the wire surface, the electric current varies along the electrode so the resistive heating term would not be constant even if the electrical resistivity were independent of temperature. The assumed Gaussian distribution for electron condensation requires the electrical current density to vary axially as

$$J(x) = \frac{\alpha i}{\sqrt{2\pi^3}\,r_w\sigma}\,\exp\left\{-\frac{(L-x)^2}{2\sigma^2}\right\} \qquad (5.8)$$

This relation must be applied with $\rho_e(T)$ in evaluating q_G'''.

If the material properties could be approximated as constant with temperature, the energy equation would become linear and, conceptually, might be solved analytically in closed form. As noted by Kays [1966], if the Peclet number is sufficiently high, the axial conduction term can be neglected and the problem would reduce to a convective thermal entry situation. The solid electrode motion corresponds to a "plug flow" for which classical solutions are available [Stein, 1966] and the surface boundary condition could probably be introduced by superposition.

Since the material properties do vary substantially with temperature (Figure 5.1), particularly across the fusion zone, an iterative numerical technique was applied via an axisymmetric version of the socalled PHOENICS code. This code is a general thermofluidmechanics computer program developed by CHAM, Ltd., from the earlier work of Patankar and Spalding [1972;

Patankar, 1980] to solve coupled sets of partial differential equations governing heat, mass and momentum transfer [Rosten, Spalding and Tatchell, 1983]. For the present work an axisymmetric version was applied to solve the thermal energy equation (5.1) alone, employing the boundary conditions and thermal properties described above. The velocity was taken as uniform at V_w throughout the field so it was not necessary to solve the momentum equations.

Some aspects of the melting phenomena were simulated by employing the "enthalpy method" [Shamsundar and Rooz, 1988; Hibbert, Markatos and Voller, 1988]. Enthalpy is taken as the dependent variable as in equation (5.1) and conversion to temperature via the property relation T(H) can account for the heat of fusion and phase transformations (e.g., γ to α) in addition to the varying specific heat of the solid. However, the velocity and boundaries of the solution region were kept fixed so convection and free surface phenomena in the molten liquid were not treated. Further, since the main interest in the present study focussed on the solid region, most of the simulations neglected the treatment of melting and phase transformation. The effect of phase transformation was tested with comparative calculations and was found negligible.

Calculations were essentially simulations of individual melting experiments. Electrode diameter was taken as 1/16 in (1.6 mm) and properties were for the material used, usually steel. The electrode extension L, wire feed speed V_w and electrical current i were as measured in the specific experiment. The quantities q_{total} and q_s were estimated from the experimental measurements via equations (5.7) and (5.5), respectively. The

resistive energy generation rate q_G was evaluated via integration and equations (5.2), (5.3) and (5.8) during the iterative solution.

A fixed numerical grid was employed. Twenty nodes were distributed uniformly in the radial direction between the centerline and the surface and eighty in the axial direction, also equidistant. The solutions were obtained via a transient approach to steady state. At each step, the enthalpy distribution was determined via the energy equation and the local temperatures and other properties were then determined from the property relationships. Iterations continued until they converged within 0.001% of the temperature at successive time steps.

Inlet temperature at the contact tip was taken as the measured room temperature, about 300K. An approximate calculation by Kim [1989] demonstrated that the convective and radiative heat losses from the electrode would be less than one per cent of the energy rate required for melting. In other preliminary calculations, numerical solutions with surface heating q_s set to zero were compared to the one-dimensional analytic solution which applies if properties are constant; the axial temperature distribution predicted numerically with allowance for property variation, agreed reasonably [Kim, Fig. 5.5, 1989].

The effect of shielding gas was introduced via the parameter α which is the fraction of energy received via electron condensation on the electrode side surface relative to the total electron condensation. Based on the experimental observations of the arc and electrode the following values were chosen:

Electrode	Gas	α
Steel	Helium, CO_2	0
Steel	Argon-2%O_2	Varied
Titanium (Ti-6Al-4V)	Argon	0
Aluminum	Argon	0

Variation of the Gaussian distribution parameter was examined [Kim, Appendix C, 1989] but a value $\sigma = 0.35$ cm was employed unless stipulated otherwise. This value was based on estimates of the radial distribution of current density in a welding plasma [Tsai, 1983].

In the regions where predicted temperatures exceeded the melting temperature the velocity was still taken as the wire feed speed V_w. Thus, possible relative motion of the molten liquid was neglected and no liquid film flow was simulated along the tapering interface observed in some experiments.

Typical predictions are demonstrated in Figure 5.2. Steel is simulated with argon shielding, electrode extension of 2.6 cm, wire feed speed of 6.6 cm/sec and electrical current of 280 amp. The nondimensional velocity is Pe $\simeq$ 14. The value $\alpha = 0.3$ is used for the electron condensation parameter in this case. Selected isotherms are plotted across a vertical centerplane of the electrode via an assumption of symmetry. Motion is vertically downward as in the experiment. The cross hatching represents the region where the temperature is predicted to exceed the melting temperature.

It is evident that outer surface heating and thermal conduction in the solid initiated the growth of a thermal boundary layer from the surface above

the 600K isotherm. As a consequence of the increased temperature near the surface, the electrical resistivity (and therefore q_G''') is increased there, raising the temperature further. This thermal boundary appears to have penetrated almost to the centerline by the second isotherm at 1000K. For comparable laminar flow in tubes, fully established Nusselt numbers are expected to require a non-dimensional distance $L^+ = (x/r_w)/Pe = 0.1$ or so without axial conduction [Kays, 1966]. For the conditions of this simulation that criterion corresponds to 0.7 diameters, but the distance for the temperature profile to become approximately invariant would be longer.

Below the melting isotherm (~ 1900K) the steel is predicted to be molten. In practice the liquid motion would depend on gravity and electromagnetic forces (accelerating forces) in relation to the wire feed speed (momentum). At low V_w one would expect a liquid film to form at the surface when $T(x,r_w) = T_m$ and to run down the solid surface, forming a taper and droplet as in the spray transfer experiments. At high V_w (therefore, high current) there may be insufficient time for the liquid film to clear so the molten region may continue to move in "solid body motion" as some cases of streaming transfer appear. The present simulation does not discriminate between these two cases; instead, it represents a form of average cylindrical equivalent to the solid plus liquid regions of the electrode with their interface falling in the interior.

Figure 5.3 presents the axial temperature profile along the electrode centerline for approximately the same situation (here $\alpha = 0.25$ and $i = 260$ amp). During the first half of the travel the temperature increases slowly due to electrical resistance heating; there is a slight increase in slope as ρ_e increases with temperature. Near $x \approx 1.4$ cm the hypothesized surface heating

begins to affect the centerline temperature. This observation corresponds to the propagation of the apparent thermal boundary layer as described above. As T approaches T_{melt} there is also a further increase due to thermal conduction upstream from the melting interface, in accordance with equation (4.6) or (4.7) evaluated near x = L (i.e., near z = 0). The upstream propagation could be estimated to be the order of $x/r_w \simeq 10/Pe$ or 0.6 mm. The near linear increase of T(x) towards the end of the electrode is likely to be a fortuitous consequence of countering effects of thermal boundary layer growth, the Gaussian increase of q''_s with x and upstream conduction.

6. DISCUSSION OF RESULTS

As noted earlier, the temperature distribution in the electrode is primarily affected by the resistive heating, heat transfer via the liquid drop and electron condensation on the cylindrical side of the electrode. Measurement of these quantities is impractical, if not impossible, so indirect methods become necessary to evaluate them. In this section the numerical technique of section 5 is applied to deduce quantitatively whether electron condensation is a reasonable explanation for the tapering of steel electrodes in argon shielding, to estimate its rate and, then, to determine the relative magnitudes of these thermal phenomena. Electron condensation on the side surface is represented by α, the ratio at the side to the total condensation on the liquid droplet plus side. In a sense, the numerical solution is used to calibrate α for the conditions of the experiments.

6.1 Effects of side electron condensation on temperature distribution

Examination of the visual observations led to the conclusion that there was

no significant electron condensation on the electrode side for aluminum or titanium alloys or for steel shielded by helium or carbon dioxide. Therefore, in these cases, $\alpha \simeq 0$. The problem becomes one-dimensional in space with uniform temperatures in the radial direction. The axial temperature distribution could be predicted by equation 4.6 if the properties did not vary significantly with temperature. To account for the property variation the numerical solution was obtained.

Figure 6.1 presents the predicted results at typical experimental conditions for these materials and shielding gases with $\alpha = 0$. A typical two-dimensional prediction for this case is included as Fig. 6.2a, demonstrating the one-dimensional isotherms or uniform radial temperature profiles. For aluminum, the low electrical resistivity yields very little resistive heating and only a slight temperature increase along the electrode. Thus, the increase to the melting point must be provided almost entirely by thermal conduction from the melting interface, comparable to the bracketed term in equation 4.6. On the other hand, the electrical resistivity of the titanium alloy is high so most of the approach to melting is due to resistive heating (Fig. 6.1b).

For steel electrodes the thermal variation of electrical resistivity is more significant, as demonstrated by the non-linear temperature variation in Fig. 6.1c with helium shielding. With carbon dioxide shielding comparable results are predicted, but the temperature is a bit higher at a given current because the wire velocity (melting rate) is less. An effect of electron condensation on the cylindrical side can be seen by comparison to Fig. 5.3 which is for $\alpha = 0.25$, simulating argon shielding. In the latter case the induced temperature rise is substantial and approaches the melting temperature

near the end of the electrode.

The predicted effect of α on the internal temperature of the electrode is demonstrated in Fig. 6.2 with variation from zero to unity (i.e., no electron condensation on the side to all on the side surface). These simulations represent steel with argon shielding with an electrical current of 280 amp. The length shown corresponds to the measured extension length. With $\alpha > 0$ the temperature profile shapes are approximately the same, appearing like the results of the near analogous thermal entry problem for flow in a tube with a heated side wall [Kays, 1966].

The plotted 1800K isotherms are approximate indications of the predicted locations of the melting interface. The extremes show that some electron condensation must occur on the side surfaces. For $\alpha = 0$ (Fig. 6.2a) the temperature does not even approach the melting point. On the other hand, for $\alpha = 1$ (Fig. 6.2d) the melting temperature is reached across the entire electrode before three-quarters of the measured length, i.e., the electrode would be much shorter than the simulation. A reasonable value predicting some surface melting, and therefore tapering, appears to fall in the range of 0.2 to 0.3 for α.

6.2 Effects of side electron condensation on energy balance

For an assumed fraction of electron condensation occurring on the side surface, the required heat transfer rate to the liquid-solid interface may be deduced by an energy balance. The experimentally measured melting rate determines the total power required. From $\rho_e(T)$ and the predicted $T(x,r)$, the energy generation rate by resistive heating may be calculated. And

integration of equation 5.5 for the specified value of α gives q_{EC}, the total input due to electron condensation on the side surface. The difference then is the required heat transfer rate through the liquid drop to the liquid-solid interface at the tip,

$$q_{L-S} = \dot{m}\,\Delta H - q_G - q_{EC}$$

where ΔH represents the energy per unit mass required to melt the electrode. Fig 6.3 shows the predicted effects on these terms of varying α for an experiment with steel at 260 amp and 2.6 cm extension.

The side surface contribution q_{EC} increases directly with α, as expected. In addition q_G increases slightly at low values of α; since the side heating increases the temperature locally, the electrical resistance and q_G increase. The required heat transfer rate to the interface q_{L-S} drops. And for $\alpha \gtrsim 0.4$ it becomes negative. That is, in conjunction with q_G a value of $\alpha \simeq 0.4$ provides enough heating to melt the electrode entirely. Any higher value is physically unrealistic for this case. Thus, the value estimated in section 6.1, $0.2 \lesssim \alpha \lesssim 0.3$, is acceptable from the energy balance viewpoint presented in Fig. 6.3.

6.3 Energy balances for differing materials

Energy balance analyses supplement the qualitative observations from examining temperature distributions as in Fig. 6.1. Predictions were made for the ranges of experimental conditions studied. Side surface electron condensation was taken as negligible ($\alpha = 0$) for each material and shielding gas except for steel with argon ($\alpha = 0.25$). Results are summarized in Fig. 6.4 and generally confirm the expectations from the temperature results.

the side heating increases the temperature locally, the electrical resistance and q_G increase. The required heat transfer rate to the interface q_{L-S} drops. And for $\alpha \gtrsim 0.4$ it becomes negative. That is, in conjunction with q_G a higher value of $\alpha \simeq 0.4$ provides enough heating to melt the electrode entirely. Any value is physically unrealistic for this case. Thus, the value estimated in section 6.1, $0.2 \lesssim \alpha < 0.3$, is acceptable from the energy balance viewpoint presented in Fig. 6.3.

6.3 Energy balances for differing materials

Energy balance analyses supplement the qualitative observations from examining temperature distributions as in Fig. 6.1. Predictions were made for the ranges of experimental conditions studied. Side surface electron condensation was taken as negligible ($\alpha = 0$) for each material and shielding gas except for steel with argon ($\alpha = 0.25$). Results are summarized in Fig. 6.4 and generally confirm the expectations from the temperature results.

For the aluminum alloy the resistive heating q_G is almost negligible and most of the required thermal energy flow is via the droplet to the liquid-solid interface q_{L-S} (Fig. 6.4a). For the titanium alloy the situation is partly reversed with the majority of the required energy being provided by q_G (Fig. 6.4b). In both cases the required value of q_G shows a break in its trend at intermediate currents; this break corresponds to the transition in melting rates and change from globular to spray mode of droplet detachment (section 3.3). These predictions emphasize the importance of the droplet behavior in the energy rate distribution as well as weld quality.

DMM/ld

With steel electrodes the balance depends strongly on the shielding gas due to its effect on the electron condensation (Fig. 6.4c, d). With helium, predicted energy balances are comparable to carbon dioxide with slight differences in the magnitudes [Kim, 1989]; about thirty percent of the required energy would be provided by resistive heating and the rest via the liquid-solid interface. With argon, predictions treating α as independent of electrical current show q_{EC} to be comparable in magnitude to q_G while the required contribution of q_{L-S} is reduced. Since α may vary with the surface area available to the arc at the tip of the electrode, and therefore with the electrical current, the magnitudes in this last simulation should be considered as illustrative rather than as an actual calibration. However, this comparison again demonstrates the importance of the energy contribution of electron condensation on the cylindrical side of the solid electrode, consistent with the temperature predictions and the visual observations.

7. CONCLUDING REMARKS

Examination of typical time scales and governing parameters, experimental observations and analyses and numerical simulations of thermal conduction in moving electrodes for GMAW have led to the following conclusions.

- Thermal conduction in the solid electrode may be approximated as a quasi-steady process except in the immediate vicinity of the periodic molten droplet.
- Droplet formation and detachment involves a number of interacting transient thermal phenomena. No significant analytical simplification was identified.
- Axial thermal conduction is primarily important only for a distance of the order of 5D/Pe from the tip where it supplies the energy necessary to supplement resistive (Joule) heating and brings the temperature to the melting point.

- Thermal conduction simulations, for steel electrodes shielded by argon gas, are quantitatively consistent with the hypothesis that electron condensation of the cylindrical side surface provides an additional energy source to form a taper at high electric currents for this combination. At 260 amp the required fraction is about twenty to thirty percent.

Table 2.1. Orders-of-magnitude of electrode time scales, steel, 1.6 mm (1/16 in) diameter

	Globular	Spray
	(Values in milliseconds)	
Droplet period	50 - 70	2-3
Electrical conduction	$< 10^{-9}$	$< 10^{-9}$
Current oscillations (60, 120, 360 Hz)	16, 8, 3	16, 8, 3
Shielding gas residence time	4	1
Viscous diffusion	2500	40
Thermal conduction	300	20
Thermal surface layer	50	3
Capillary waves	30	30
Surface oscillation	16	2
Thermocapillary (Marangoni):		
a) significant velocity change	60	4
b) surface velocity $\simeq V_w$	4	0.3
c) residence time based on dT/dx	2	0.4
d) residence time for induced flow	60	20

DNM/ld

Table 3.1. The combination of welding parameters used in experiments.

	Shielding gas			Electrode extension (mm)	Arc gap (mm)	Welding current (amp)
	Argon	Helium	CO_2			
Mild steel	x	x	x	16,26,36	14: Ar 6: He 8: CO_2	180-420
Aluminium(1100, 5356)	x			16,26,36	14: Ar	80-220
Ti-6Al-4V	x		x	16,26,36	14: Ar	120-260

x = welding was performed.

DHM/ld

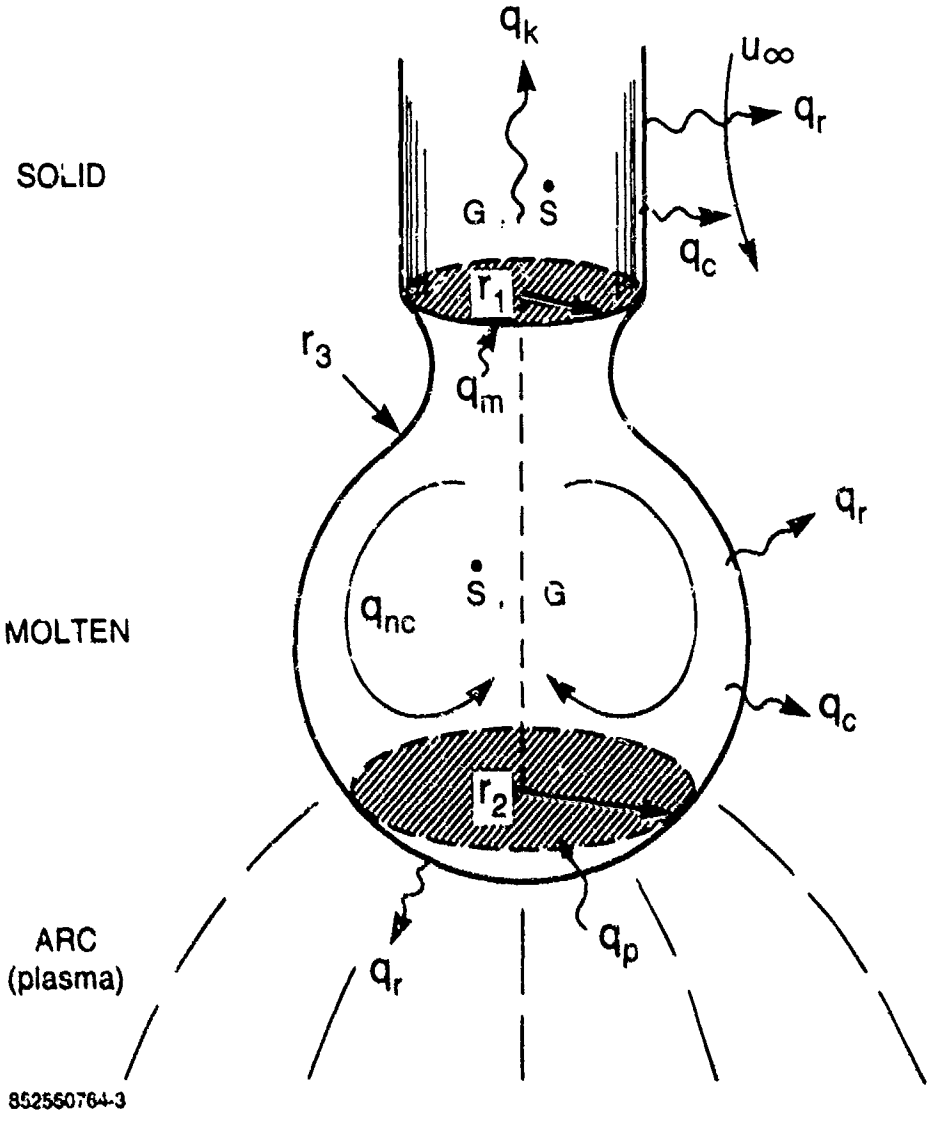

Figure 1.1. Possible thermal processes in an idealized vertical droplet and electrode.

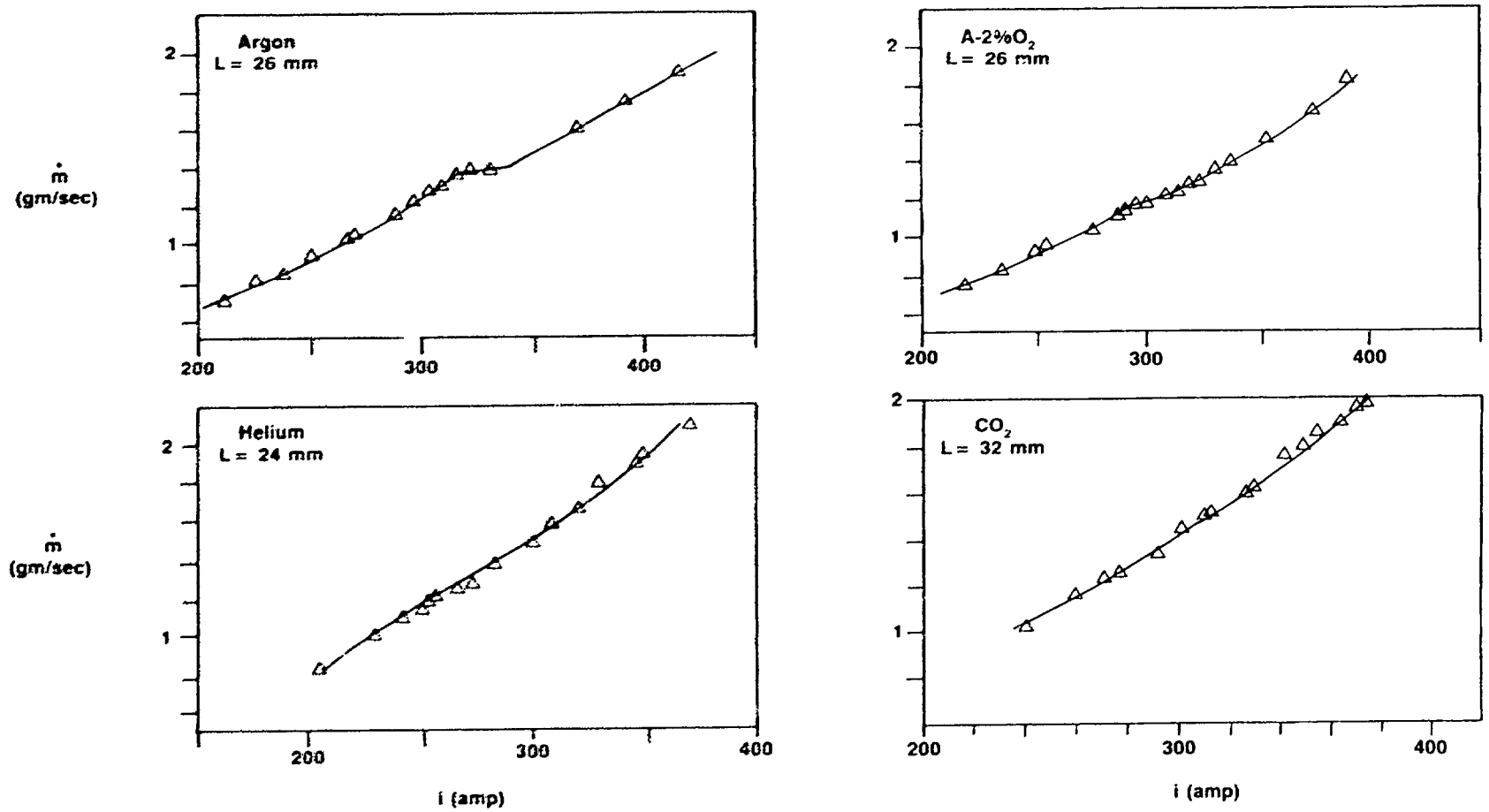

Figure 3.1. Melting rate measurements with 1.6 mm steel electrodes.

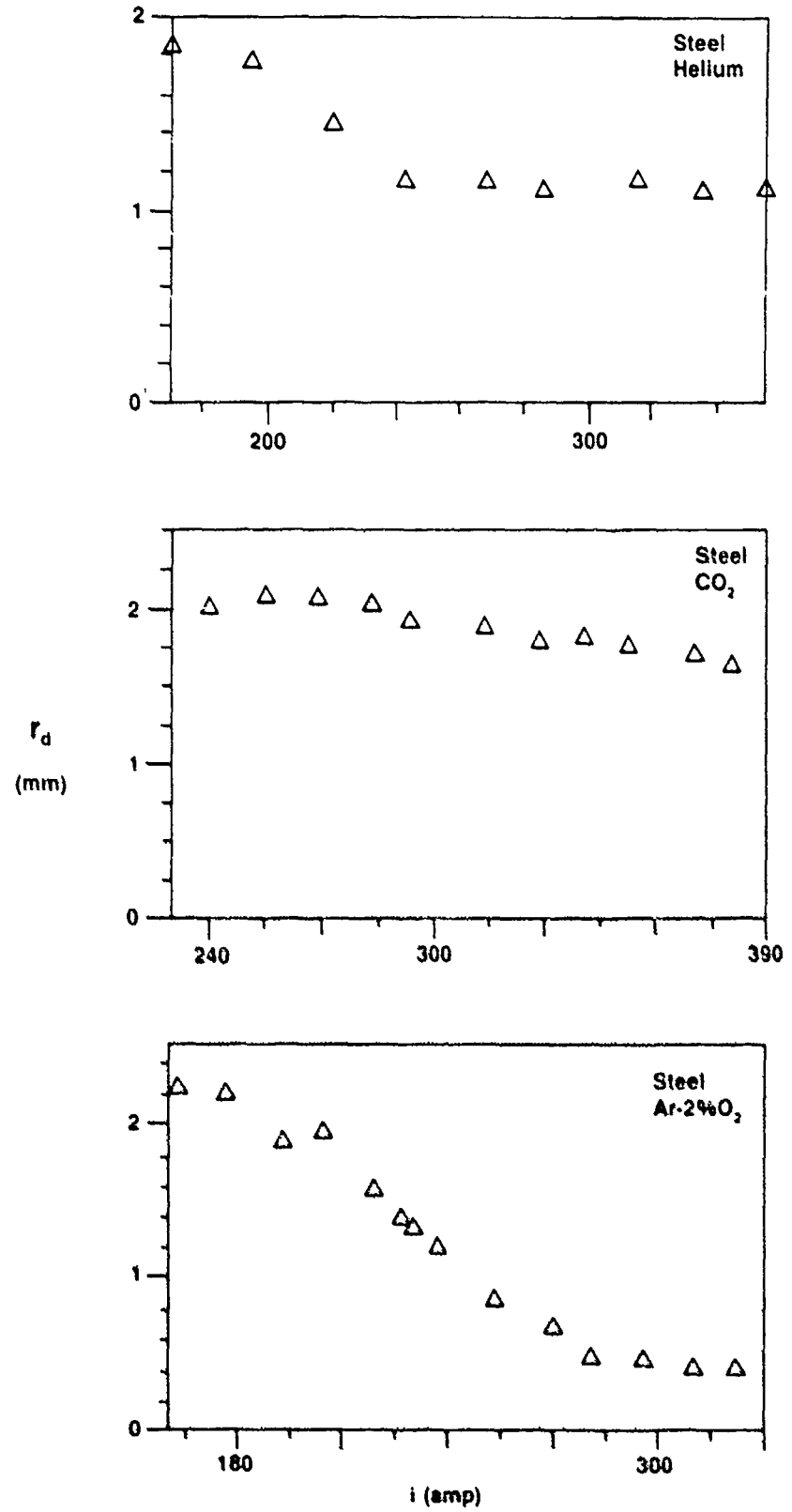

Figure 3.2. Effect of shielding gas on droplet size, steel electrodes.

89254:384-2

Figure 3.3. Effect of electrical current on metal transfer process for steel electrodes with argon shielding.

Ti-6Al-4V
Globular

Steel
Globular

Steel
Streaming

892541084-11

Figure 3.4. Current path indications with argon shielding.

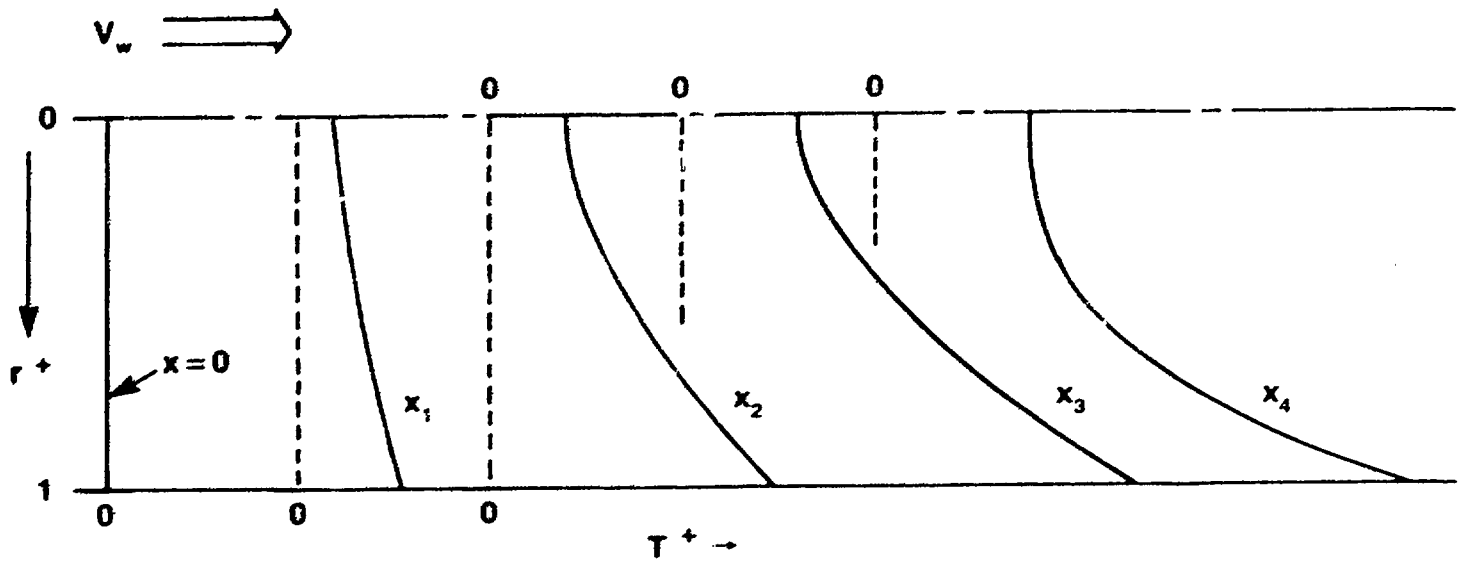

Figure 4.1. Qualitative simulation of wire temperature distribution for electron condensation increasing toward molten tip.

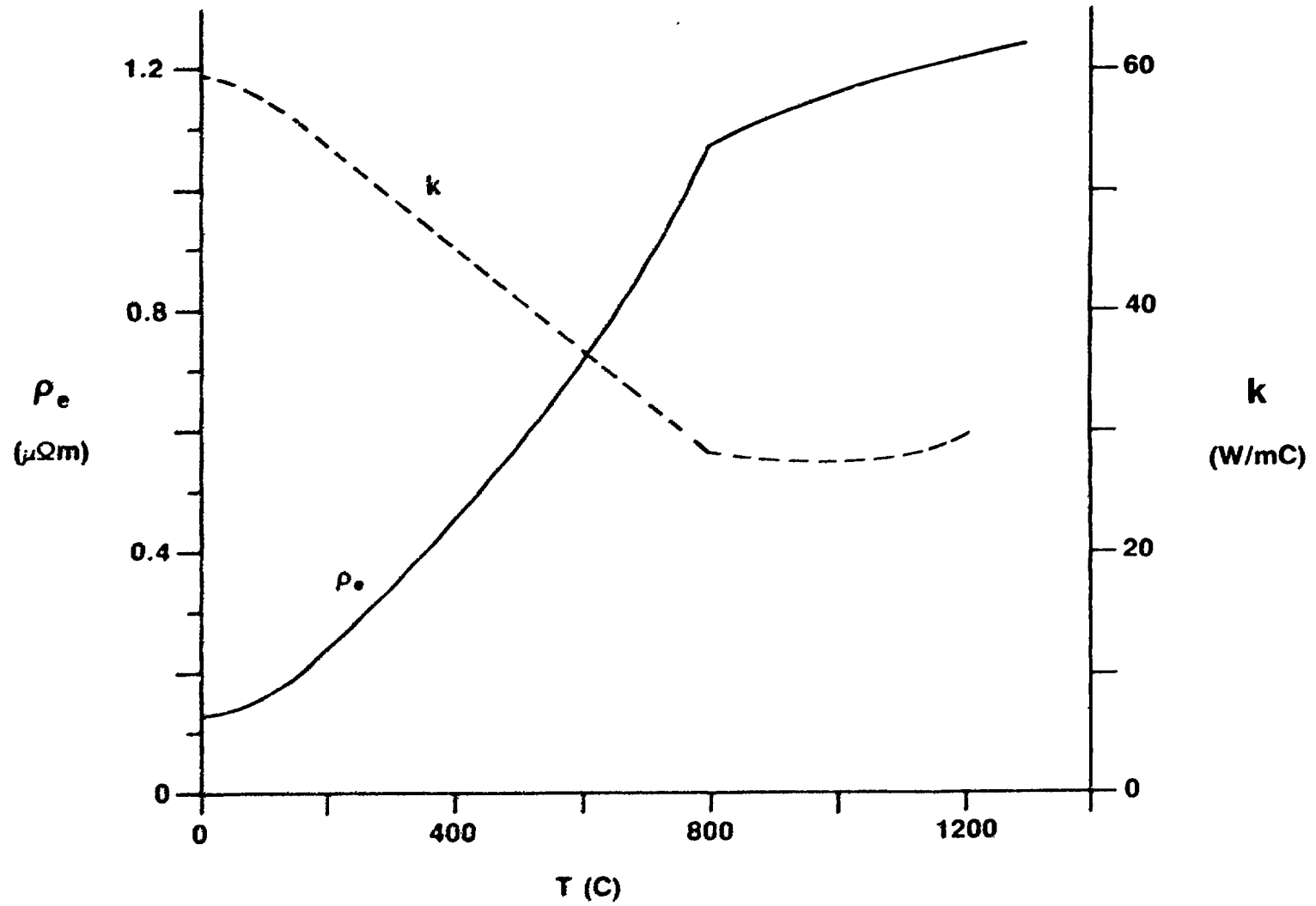

Figure 5.1. Thermal variation of electrical resistivity and thermal conductivity of AISI-SAE Grade 1008 steel (Metals Handbook, 1979).

892541084-4

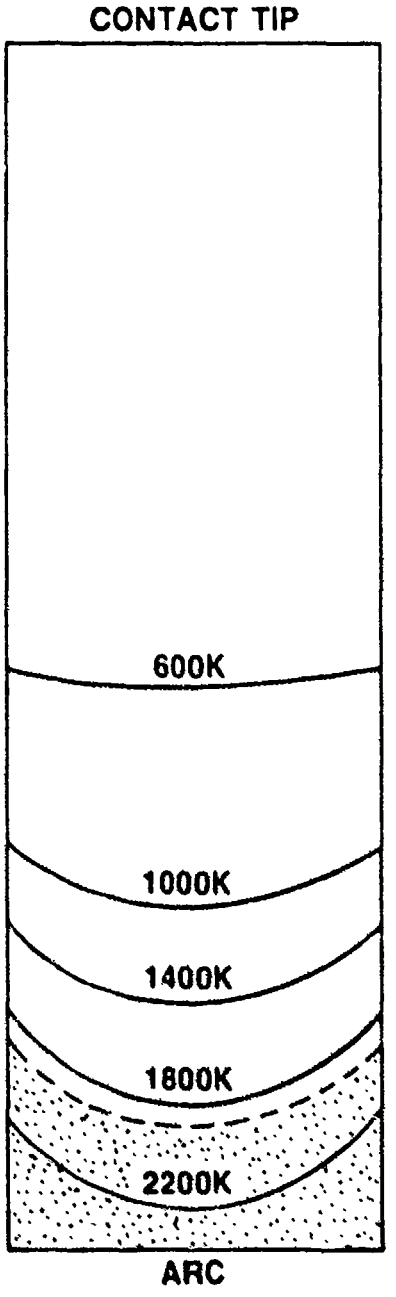

Figure 5.2. Typical temperature distribution in the electrode as predicted by the PHOENICS code, α = 0.3, I = 280 amp.

892541084-5

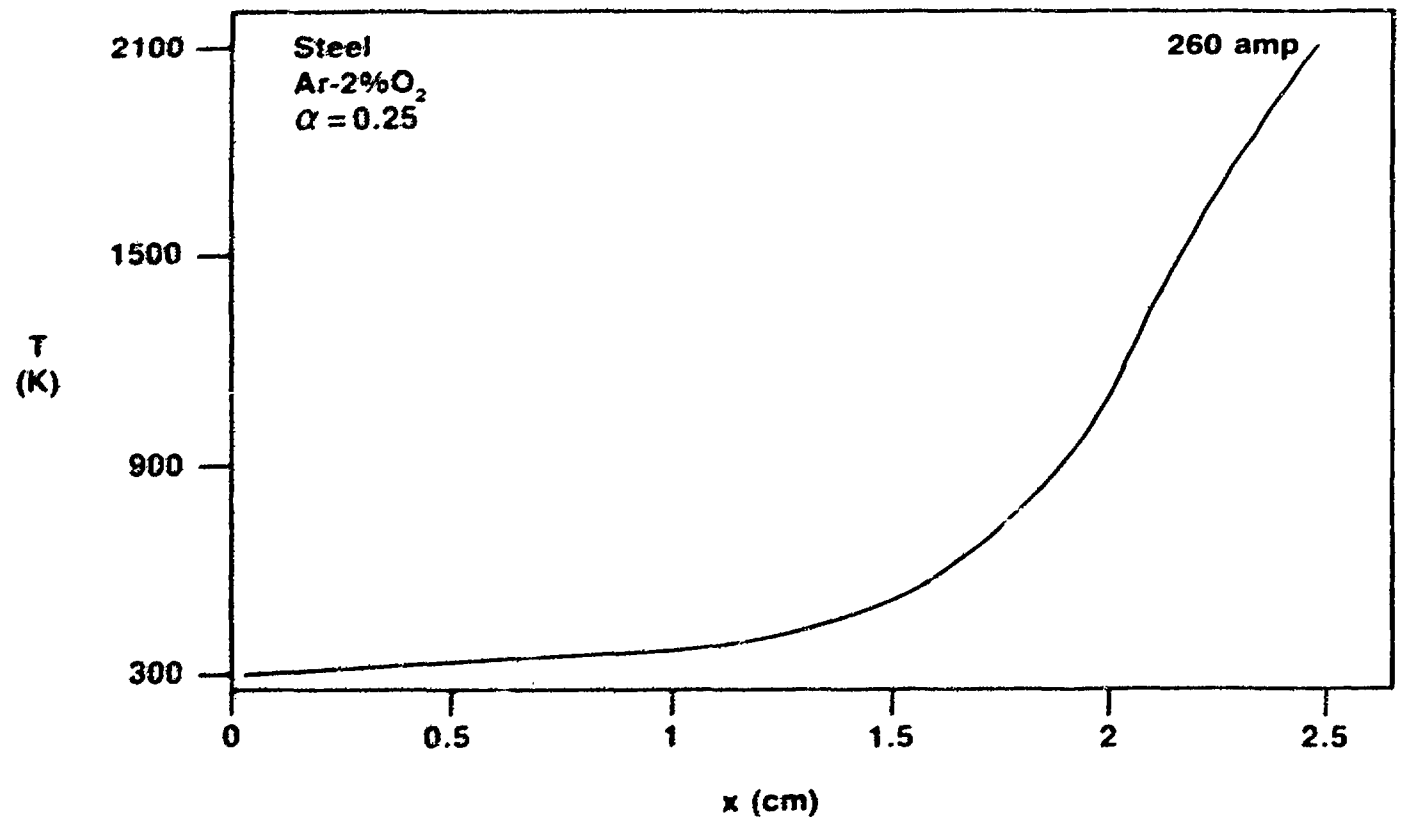

Figure 5.3. Axial temperature distribution along electrode centerline as predicted by PHOENICS code.

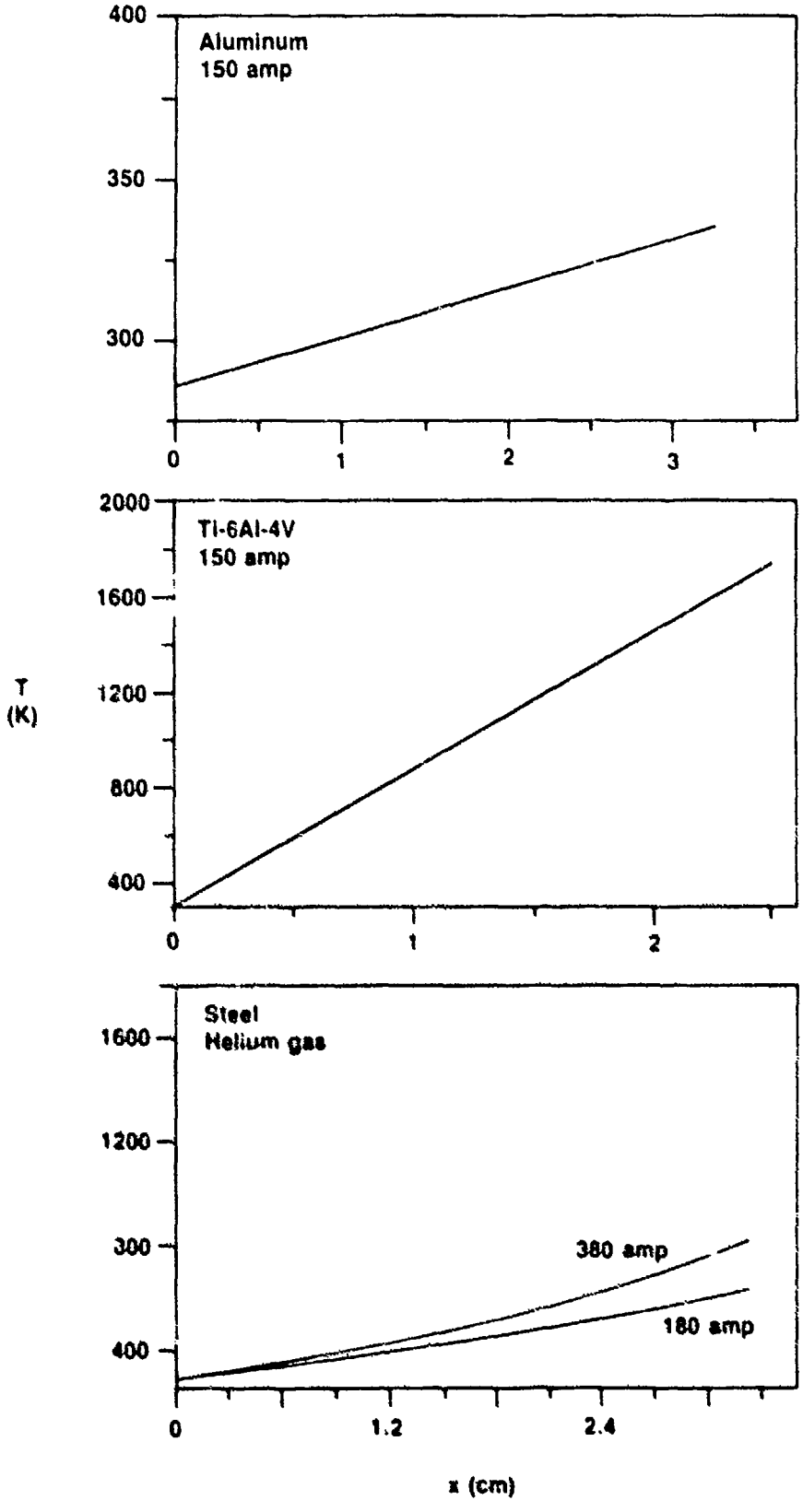

Figure 6.1. Predicted axial temperature distribution with negligible electron condensation on side surface ($\alpha \cong 0$).

692541084-7

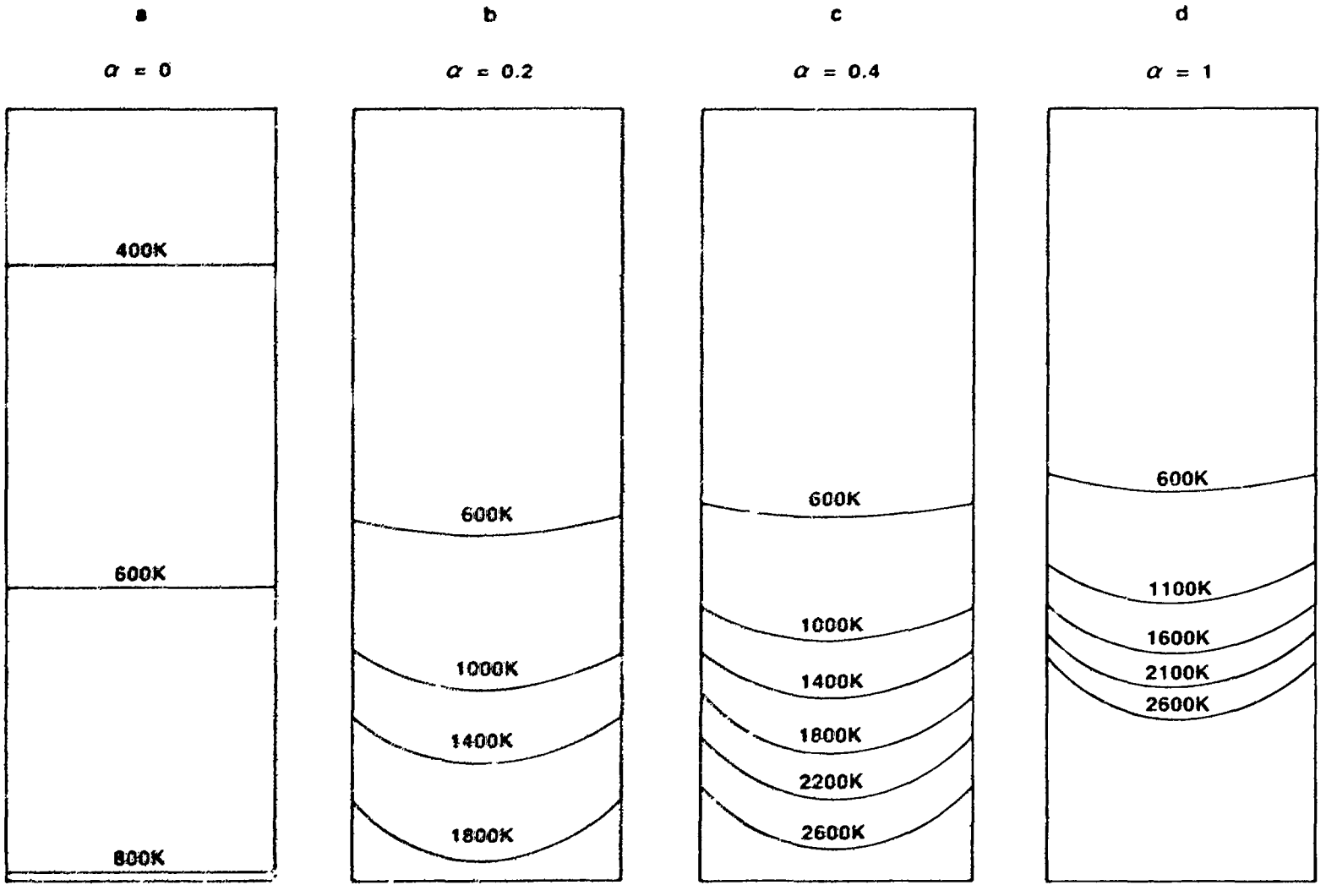

Figure 6.2. Predicted effect of electron condensation on side surface of solid electrode.

692541084 8

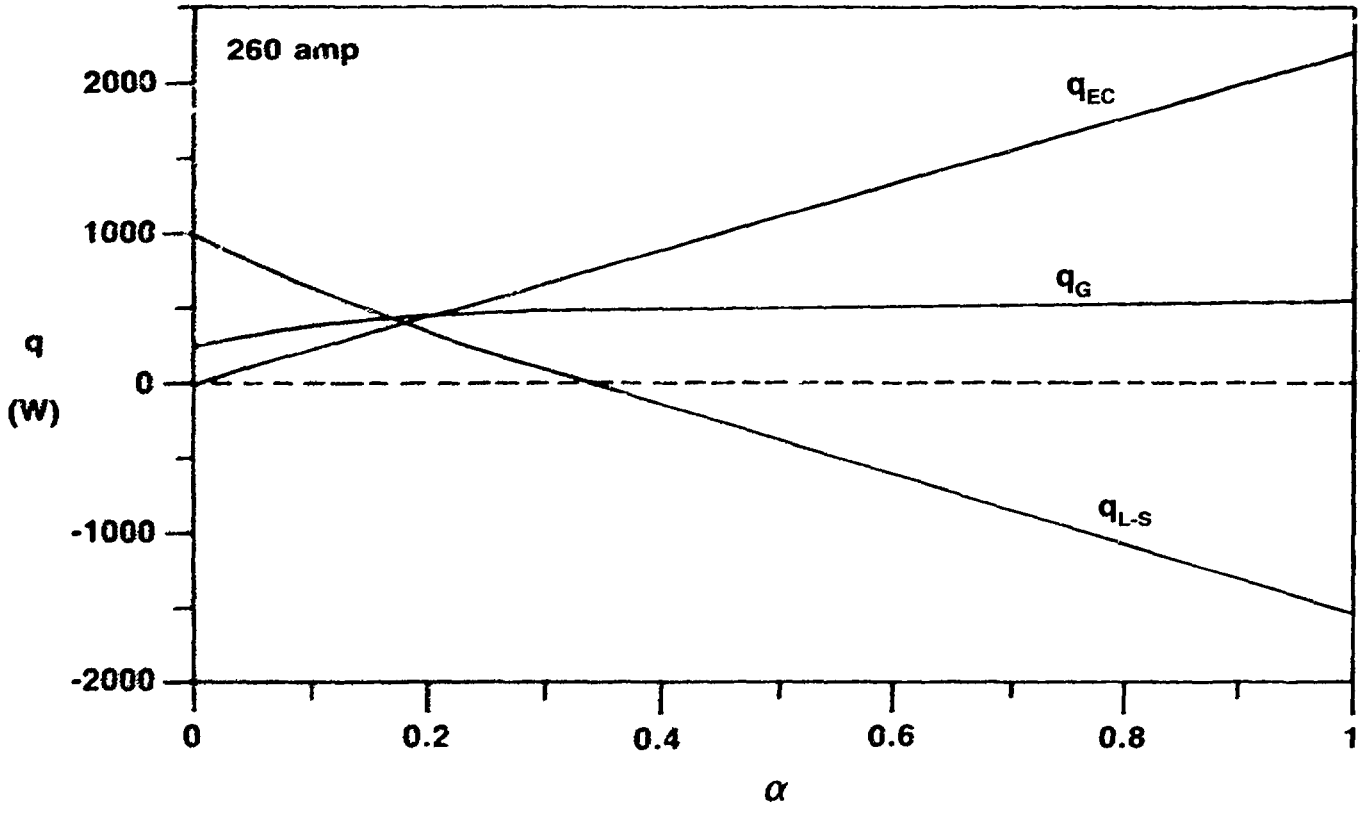

Figure 6.3. Predicted effects of electron condensation ratio α on thermal energy balance for steel electrodes with argon shielding.

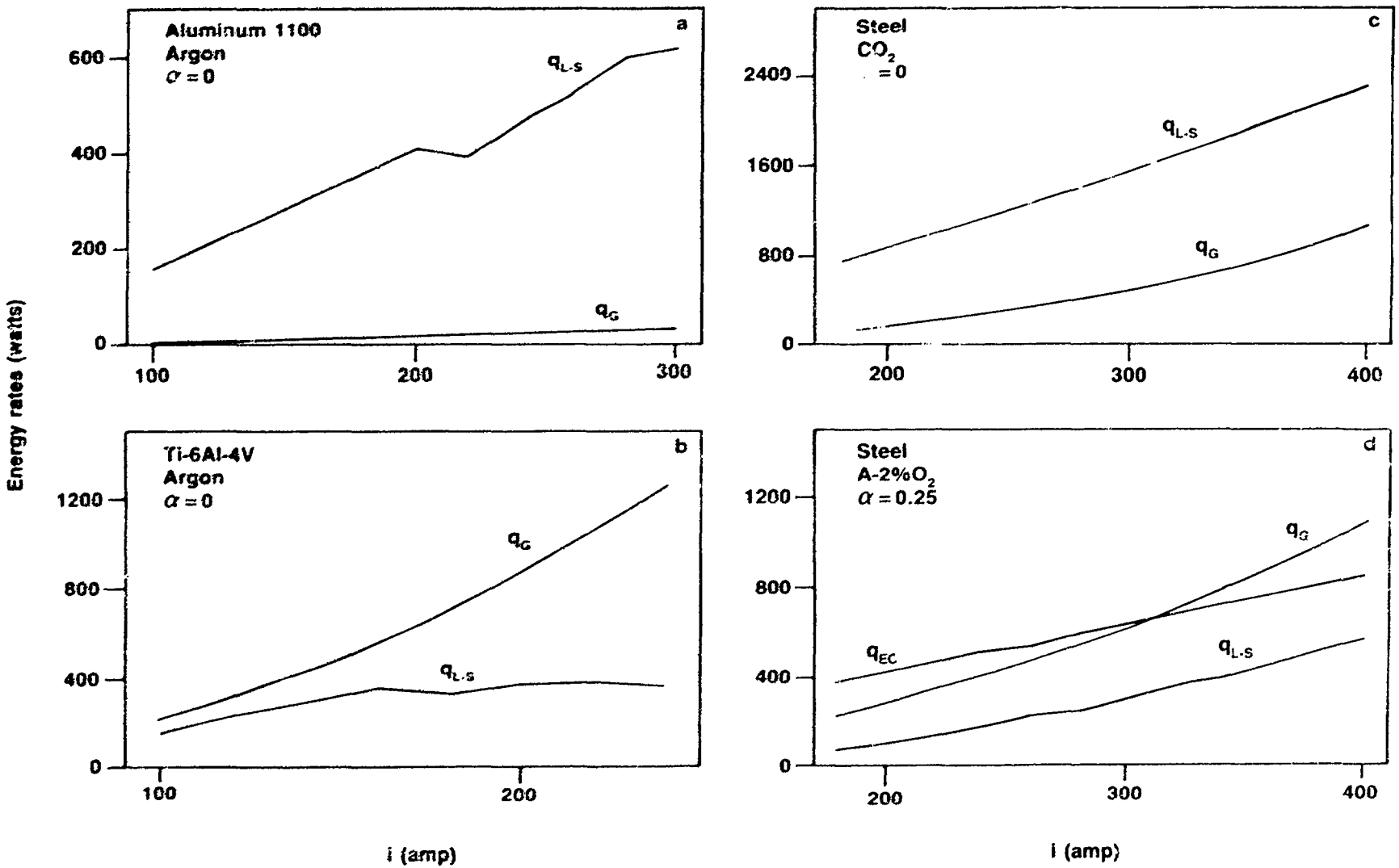

Figure 6.4. Predicted thermal energy balances for various electrode materials.

Appendix B. CLASSICAL EIGENVALUE SOLUTION FOR THERMAL CONDUCTION IN IDEALIZED MOVING ELECTRODE

by

J.S. Uhlman, Jr.[1] and D.M. McEligot

1. INTRODUCTION

Recent visualization studies of metal transfer by Kim [1989; Kim, McEligot and Eagar, 1989] showed apparent current paths with the arc attaching on the cylindrical side surface of steel electrodes with argon shielding. He hypothesized that this indicated that a portion of the electrons condensed on the side surface, liberating heat of condensation there which led to side surface melting, liquid film convection and taper formation. Kim modeled the process approximately with the commercial PHOENICS code [Rosten, Spalding and Tatchell, 1983] with internal resistive heating plus heating from the outer cylindrial surface and concluded that the results quantitatively supported his hypothesis.

With suitable idealizations, the problem can be analysed by classical techniques and a useful closed form solution can evolve. The idealized situation is analogous to transient thermal conduction in an infinite cylindrical rod [Carslaw and Jaeger, 1959] and thermal entry problems for

---

1. Naval Underwater Systems Center, Newport, RI 02841. Formerly Hydrothermodynamics Research Dept., Gould Ocean Systems Division (now Westinghouse Naval Systems Division) Middletown, RI 02840

DMH/ld

internal convection to a "plug" flow inside a circular tube [Kays, 1966; Stein, 1966]. By applying the method of superposition [Hildebrand, 1962] one can obtain the internal temperature distribution for arbitrary variation of the surface heating on moving electrodes. The results can be applied to estimate the distance from the contact tip to the start of surface melting as well to test numerical analyses as by Kim to develop confidence in their predictions.

The objective of the present work is to develop an exact solution for the idealized problem of thermal conduction in a moving electrode in order (1) to predict the beginning of melting on the side surface and (2) to provide bases for verifying most features of numerical predictions.

2. MATHEMATICAL STATEMENT OF THE PROBLEM

The governing thermal energy equation for steady motion of a solid electrode can be written in cylindrical coordinates as [Kays 1966]

$$\rho V \frac{\partial H}{\partial x} = \frac{\partial}{\partial x}\left(k\frac{\partial T}{\partial x}\right) + \frac{1}{r}\frac{\partial}{\partial r}\left(kr\frac{\partial T}{\partial r}\right) + q_G''' \qquad (2.1)$$

under the idealization of rotational symmetry. Here the axial coordinate x increases in the direction of motion from contact tip towards the melting interface and V is the uniform axial velocity. The quantity q_G''' represents the volumetric energy source due to resistive heating by the electrical current and H is the specific enthalpy. (If the specific heat can be approximated as constant, the first term may be written as $\rho V c_p \partial T/\partial x$.)

Appropriate boundary conditions for an electrode with electron condensation occurring on the side surface as well as the end, but with no significant

radiative or convective heat transfer to the surroundings, would be

$$\text{Initial:} \qquad T(0,r) = T_{in} \tag{2.2a}$$

$$\text{Center line:} \qquad \frac{\partial T}{\partial r}(x,0) = 0 \tag{2.2b}$$

$$\text{Side surface:} \qquad q_s''(x) = -k\frac{\partial T}{\partial r}(x,r_w) = \text{specified fn}(x) \tag{2.2c}$$

$$\text{End:} \qquad q_e'' = -k\frac{\partial T}{\partial x}(L,r) = \text{specified fn}(r) \tag{2.2d}$$

This problem is essentially the one that Kim [1989; Kim, McEligot and Eager, 1989] solved numerically for q_e'' = constant.

As an approximation, we consider the material properties ρ, c_p, k and ρ_e, to be constant; some appropriate average values would be employed in application of the results. Non-dimensional variables may be defined as

$$\bar{T} = (T - T_{in})/T^*, \qquad \bar{q}_G = q_G''' r_w^2/(kT^*)$$

$$\bar{x} = (2x/r_w)/Pe \qquad \text{and} \qquad \bar{r} = (r/r_w)$$

where Pe is the Peclet number, Vd_w/α, and T^* is a reference temperature to be chosen for convenience. Using these definitions, one may rearrange the energy equation to

$$\frac{\partial \bar{T}}{\partial \bar{x}} = \frac{4}{Pe^2}\frac{\partial^2 \bar{T}}{\partial \bar{x}^2} + \frac{1}{\bar{r}}\frac{\partial}{\partial \bar{r}}\left(\bar{r}\frac{\partial \bar{T}}{\partial \bar{r}}\right) + \bar{q}_G \tag{2.2}$$

For Pe $\tilde{>}$ 100 the axial conduction term involving the Peclet number can be neglected relative to the others [Schneider, 1957]. Further, if one examines the one-dimensional solution of the energy equation [Kim, McEligot and Eagar, 1989], one finds the upstream axial diffusion from the end becomes negligible beyond a distance $\Delta x/D \approx 5/Pe$.

DMM/ld

Typical values of the Peclet number for GMA Welding of steel are in the range of 4 to 40 or so for globular to spray conditions or from low to high electrical currents. The end heating consequently does not affect the region of interest for the present work and, though not miniscule, the axial conduction from other sources can be expected to be small. Therefore, we simplify the thermal energy equation to the form

$$\frac{\partial \bar{T}}{\partial \bar{x}} = \frac{1}{\bar{r}} \frac{\partial}{\partial \bar{r}} \left(\bar{r} \frac{\partial \bar{T}}{\partial \bar{r}} \right) + \bar{q}_G \qquad (2.3)$$

This equation has the same form as the governing equation for transient, one-dimensional thermal conduction which has been studied extensively [Boelter et al., 1965; Özisik, 1980], so in many cases existing solutions may be adopted directly [Schneider, 1957].

To be unique, the solution to this equation must be constrained by an inlet (initial) condition and two boundary conditions (and specification of $\bar{q}_G(\bar{x},\bar{r})$). In non-dimensional terms these may be written from equations (2.2) as

$$\begin{aligned} &\text{Initial:} && T(0,\bar{r}) = 0 \\ &\text{Centerline:} && \frac{\partial \bar{T}}{\partial \bar{r}}(\bar{x},0) = 0 \\ &\text{Side surface:} && \frac{\partial \bar{T}}{\partial \bar{r}}(\bar{x},1) = -\frac{q_s''(x) r_w}{kT^*} = -\frac{q_s''(x)}{|q_r''|} = \bar{q}_s(\bar{x}) \end{aligned} \qquad (2.4)$$

where T^* is defined as $|q_r''| r_w/k$ and q_r'' is a reference value of the surface heat flux. It should be noted that the positive direction for heat flux is in the direction of increasing radius, i.e., outward, and $\bar{q}_s$ has been defined to be positive when heating is from the outside. A peak or average magnitude of $q_s''(x)$ could be appropriate for q_r''. With constant heat flux from outside, $\bar{q}_s$ becomes unity and positive.

Choosing T^* also establishes the definition of $\bar{q}_G$, the non-dimensional

volumetric energy generation rate. It becomes

$$\bar{q}_G = \frac{q_G''' r_w^2}{kT^*} = \frac{q_G''' r_w}{q_r''} \tag{2.5}$$

and thus its value is dependent on the choice of the reference value for the surface heat flux. For resistive heating,

$$q_G''' = J^2 \rho_e = i^2 \rho_e / (\pi r_w^2)^2$$

provided the electrical current density is taken as uniform across the cross section.

3. GENERAL SOLUTION

For this section the overbars representing non-dimensionalization will be suppressed for convenience, unless needed for clarity. Thus, the symbols T, r, x, q_G and q_s will all represent their non-dimensional versions as defined above.

3.1 Constant energy source on side surface

A basic solution for a constant surface heat flux is first required, i.e., a step change to $(\partial T/\partial r) = +1$ at $x = 0$ and $r = 1$. We separate $T(x,r)$ into two components (one to accomodate the continuous increase in temperature level due to q_G), $T(x,r) = T_1(x,r) + T_2(x)$, where their respective governing equations become

$$\frac{\partial T_1}{\partial x} = \frac{1}{r} \frac{\partial}{\partial r}\left(r \frac{\partial T_1}{\partial r}\right) \tag{3.1}$$

and

$$\frac{\partial T_2}{\partial x} = q_G \tag{3.2}$$

The solution of the second is $T_2 = q_G x + C$ with $C = 0$ from the initial condition at $x = 0$.

DMM/ld

With a bit of experimentation, T_1 is separated further to

$$T_1(x,r) = \tau(x,r) + 2x + \frac{1}{2} r^2 \qquad (3.3)$$

in order to develop a problem statement with homogeneous radial boundary conditions. The second term on the right accounts for the increase in average temperature level due to surface heating and the last term provides the asymptotic radial profile at large x. The appropriate partial derivative of $\tau(x,r)$ is

$$\frac{\partial \tau(x,0)}{\partial r} = \frac{\partial T_1(x,r)}{\partial r} - r$$

so its boundary conditions become

$$\frac{\partial \tau(x,0)}{\partial r} = \frac{\partial T_1(x,0)}{\partial r} = 0$$

$$\frac{\partial \tau(x,1)}{\partial r} = \frac{\partial T_1(x,1)}{\partial r} - 1 = 0$$

Its governing equation is the same form,

$$\frac{\partial \tau}{\partial x} = \frac{1}{r} \frac{\partial}{\partial r} \left(r \frac{\partial \tau}{\partial r} \right)$$

and the initial condition becomes

$$\tau(0,r) = T_1(0,r) - \frac{1}{2} r^2 = -\frac{1}{2} r^2$$

The general solution to this problem via separation of variables is

$$\tau(x,r) = A_0 + A_\gamma e^{-\gamma^2 x} J_0(\gamma r) \qquad (3.4)$$

with the derivative

$$\frac{\partial \tau(x,r)}{\partial r} = -A_\gamma \gamma e^{-\gamma^2 x} J_1(\gamma r)$$

DMM/ld

The boundary conditions can be satisfied with eigenvalues γ_k such that

$$J_1(\gamma_k) = 0 \qquad \text{for } k = 1,2,.....$$

Özisik [1980] provides the first ten roots of $J_1(z) = 0$ and they are repeated here as γ_k in Table 3.1. The initial condition implies that $A_o = 0$, so the solution can be written

$$\tau(x,r) = \sum_{k=1}^{\infty} A_k e^{-\gamma_k^2 x} J_o(\gamma_k r) \tag{3.5}$$

and further requires

$$-\frac{1}{2} r^2 = \sum_{k=1}^{\infty} A_k J_o(\gamma_k r)$$

Via equations (11.4.5) and (11.4.10) of Abramowitz and Stegun [1964] one can show this condition leads to the evaluation

$$A_k = -\frac{1}{\gamma_k}\left[J_1(\gamma_k) - \frac{2}{\gamma_k} J_2(\gamma_k)\right] \Big/ J_o^2(\gamma_k)$$

or

$$A_k = -\frac{2}{\gamma_k^2 J_o(\gamma_k)} \tag{3.6}$$

since $J_1(\gamma_k) = 0$. The values of these eigenconstants have been calculated with a subroutine AJ0(X) based on equations provided by Abramowitz and Stegun and are also listed in Table 3.1.

The solution for the constant surface heat flux is then

$$T_1(x,r) = T_{cq}(x,r) = 2x + \frac{r^2}{2} + \sum_{k=1}^{\infty} A_k e^{-\gamma_k^2 x} J_o(\gamma_k r) \tag{3.7}$$

where the subscript "cq" is a reminder that it applies to this basic solution.

DMM/ld

3.2 Axial variation of surface energy source

For a variable surface heat flux $q_s''(x)$, such that $q_s = q_s(x)$ rather than unity, the method of superposition [Hildebrand, 1962, p. 452] gives the the temperature distribution as

$$T_1(x,r) = q_s(0)T_{cq}(x,r) + \int_0^x T_{cq}(x-\xi,r)\frac{dq_s}{d\xi}(\xi)d\xi \qquad (3.8)$$

An alternate representation may be obtained by integrating by parts and noting that $T(0,r) = 0$. It takes the form

$$T_1(x,r) = \int_0^x q_s(\xi)\,\frac{\partial T_{cq}}{\partial x}(x-\xi,r)\,d\xi$$

However, it is anticipated that convergence of the series in this second form would be slow [Bankston and McEligot, 1969].

Substitution of equation (3.7) into (3.8) and integration yields the overall relationship needed for varying surface heat flux in terms of the eigenvalue representation,

$$T(x,r) = \frac{r^2}{2}\,q_s(x) + 2\int_0^x q_s(\xi)d\xi + \sum_{k=1}^{\infty} A_k e^{-\gamma_k^2 x} J_o(\gamma_k r)\left\{ q_s(0) + \int_0^x e^{\gamma_k^2 \xi}\left(\frac{dq_s}{d\xi}(\xi)\right)d\xi\right\} + q_G x \qquad (3.9)$$

The reader is reminded that the quantities shown are the non-dimensional versions as defined above. Values of A_k and $J_o(\gamma_k)$ are listed in Table 3.1.

4. DISCUSSION AND APPLICATION

For treatment of electron condensation along the cylindrical side surface

of an electrode, an appropriate representation of $q''_s(x)$ must be chosen and equation (3.9) must then be integrated. The integration could be done numerically, but for convenience of application and for physical insight it is worth while to choose approximating functions which are easily integrable so a result may be obtained in closed form. One such function is the Gaussian distribution chosen by Kim [1989],

$$q''_s(x) = \frac{\alpha i V_c}{\pi r_w} \cdot \frac{1}{\sigma\sqrt{2\pi}} \exp\left\{-\frac{(L - x)^2}{2\sigma^2}\right\} \qquad \text{at } r = r_w \qquad (4.1)$$

but, since its range extends to $x = -\infty$, it would be a bit awkward to apply (e.g., one must account for the implied heating before the electrode reaches the contact tip).

Typical functions which can be adjusted to approximate Kim's distribution, with a maximum at a chosen location $x = L$ and zero at a point where the electron condensation can be considered negligible, are

a) linear, $q''_s = q_o \eta$

b) polynomials

c) sinusoids, $q''_s(\eta) = q_o \sin(m\eta)$

d) exponentials [Reynolds, 1968]

$$q''_s(\eta) = q_o (1 - e^{-m\eta})$$

The location $\eta = 0$ would be chosen at an appropriate value of x. For lesser values of x, $q_s = 0$ and the problem would be one-dimensional according to the idealizations employed above.

In order to predict approximately the location where surface melting is expected, one should evaluate equation (3.9) for non-dimensional $r = 1$ to determine the distance to reach T_{melt}. Then the first term becomes

$q_s(x)/2$. The coefficient in the last term is $A_k J_o(\gamma_k) = -2/\gamma_k^2$ from equation (3.6); this quantity is also listed in Table 3.1 for convenience. One can perform this estimation as a two step process: (1) calculate the value of the one-dimensional temperature $T_2 = q_G x_o$ at the location where appreciable side heating starts x_o, then (2) apply equation (3.9) with T_{in} determined from $T_2(x_o)$ in defining non-dimensional T(x,1). Two countering effects serve to reduce the inaccuracy in this approximation. While $\rho_e(T)$ increases with T for steel (instead of remaining constant as assumed in the idealized solution), current density J(x) decreases with x as $q_s''(x)$ increases. Consequently their product

$$\bar{q}_G = q_G''' r_w \Big/ q_r'' = J^2 \rho_e r_w \Big/ q_r''$$

varies less than it might. A linear relationship may provide a first approximation for $q_s(x)$ and will ease the integration required for equation (3.9).

The present solutions may be used to verify codes for thermal conduction in electrodes. Although this closed form treatment cannot be extended easily to variable material properties in order to test numerical prediction for the same problem, computer codes can be constrained to constant properties for an exact comparison. If the code includes treatment of axial thermal conduction, the idealizations of the closed form result (equation (3.9)) will be approached by performing the computer calculations for high electrode feed speeds so the Peclet number is large.

DNM/ld

Table 3.1 Eigenvalues and eigenconstants for basic solution for constant surface heat flux

k	γ_k	A_k	$J_o(\gamma_k)$	$A_k J_o(\gamma_k) = -2/\gamma_k^2$
1	3.8317	0.338221	-0.402759	-0.136221
2	7.0156	-0.135397	0.300115	-0.0406350
3	10.1735	0.0773859	-0.249704	-0.0193236
4	13.3237	-0.0515950	0.218359	-0.0112662
5	16.4706	0.0375253	-0.196465	-0.00737244
6	19.6159	-0.0288661	0.180063	-0.00519773
7	22.7601	0.0230932	-0.167184	-0.00386084
8	25.9037	-0.0190181	0.156724	-0.00298062
9	29.0468	0.0160154	-0.148011	-0.00237046
10	32.1897	-0.0137275	0.140605	-0.00193017

REFERENCES CITED

Allemand, C.D., R. Schoeder, D.E. Ries and T.W. Eagar, Welding J., 64, pp. 45-47.

Allum, C.J., 1985a. J. Phys. D: Appl. Phys.,18 pp. 1431-1446.

Allum, C.J., 1985b. J. Phys. D: Appl. Phys.,18 pp. 1447-1468.

ASM, 1979. Metals handbook, 9th. Ed., American Society of Metals

Block-Bolten, A., and T.W. Eagar, 1984. Met. Trans. B, 15B, pp. 461-469.

Boelter, L.M.K., V.H. Cherry, H.A. Johnson and R.C. Martinelli, 1965. Heat transfer notes. New York: McGraw-Hill.

Clift, R., J.R. Grace and M.E. Weber, 1978. Bubbles, drops and particles. New York: Academic.

Cooksey, C.J., and Miller, D.R., 1962. Metal transfer in gas-shielded arc welding, Physics of the Welding Arc--A Symposium 1962, pp. 123-132.

Eager, T.W., 1989. An Iconoclast's view of the physics of welding - Rethinking old ideas. 2nd. Int. Conf. on Trends in Welding Research, ASM International, Gatlinburg.

Eager, T.W., 1987. Personal Communication, M.I.T., 5 Nov.

Eichhoff, S.T., 1988. M.S. thesis, M.I.T.

Greene, W.J. 1960. Trans. AIEE,.79, pp 194-203.

Halmoy, E., 1980. Wire melting rate, droplet temperature and effective anode melting potential. Arc Physics and Weld Pool Behavior, Cambridge: Welding Inst., pp. 49-57.

Heiple, C.R. and J.R. Roper, 1982. Welding J., 61, pp. 97s-102s.

Hibbert, S.E., N.C. Markatos and V.R. Voller, 1988. Int. J. Heat Mass Transfer, 31, pp. 1785-1795.

Kays, W.M., 1966. Convective heat and mass transfer. New York: McGraw-Hill.

Kim, Y.-S., 1989. Metal transfer in gas metal arc welding. Ph.D. thesis, M.I.T.

Kim, Y.-S., 1987. Personal analysis notes. M.I.T.

Kuo, S., and Y.H. Wang, 1986. Welding J., 65, pp 63s-70s.

Kreith, F., 1973. Principles of heat transfer. Scranton: Intext.

REFERENCES CITED (Cont'd.)

Lai, C.L., S. Ostrach and Y. Kamotani, 1985. The role of free-surface deformation in unsteady thermocapillary flow. U.S.-Japan Heat Transfer Joint Seminar.

Lamb, H., 1932. Hydrodynamics, 6th. ed. Cambridge Univ. Press.

Lancaster, J.F., ed., 1984. The physics of welding. Oxford: Pergamon.

Lesnewich, A., 1958a. Welding J., 37, pp 343s-353s.

Lesnewich, A., 1958b. Welding J., 37, pp 418s-425s.

Lesnewich, A., 1987. Welding J., 66, pp 386s-387s.

McEligot, D.M., and J.S. Uhlman, 1988. Metal transfer in Gas Metal Arc Welding. Tech. report, Westinghouse-O/NPT-723-HYDRO-CR-88-01, ONR contract N00014-87-C-0668.

Morris, R.A., 1989. Personal communication, David Taylor Research Center, Annapolis.

Needham, J.C., and Carter, A.W., 1965. British Welding, pp. 229-241.

Oreper, G.M., T.W. Eagar and J. Szekely, 1983. Welding J., 62, pp 307s-312s.

Patankar, S.V., 1980. Numerical heat transfer and fluid flow. Washington: Hemisphere.

Patankar, S.V., and D.B. Spalding, 1972. Int. J. Heat Mass Transfer, 15, pp. 1787-1805

Pimputkar, S.M., and S. Ostrach, 1980. Phys. Fluids, 23, pp. 1281-1285.

Reynolds, H.C., 1968. Ph.D. thesis, Univ. Arizona.

Reynolds, H.C., T.B. Swearingen and D.M. McEligot, 1969. J. Basic Engr., 91, pp. 87-94.

Rosten, H.I., D.B. Spalding and D.G. Tatchell, 1983. Proc., 3rd. Int. Conf. Engr. Software, pp. 639-655.

Schneider, P.J., 1957. Trans., ASME, 79, pp. 765-773.

Shamsundar, N., and E. Rooz, 1988. Handbook of numerical heat transfer (Ed.: W.J. Minkowycz et al.), New York: Wiley, Ch. 18, pp. 747-786.

Sozou, C., and W.M. Pickering, 1975. J. Fluid Mech., 70, p. 509.

Stein, R.P., 1966. Adv. Heat Transfer, 3, pp. 101-174.

Tsai, N.S., 1983. Ph.D. thesis, M I T.

REFERENCES CITED (Cont'd.)

Ueguri, S., K. Hara and H. Komura, 1985. Welding J., 64 pp. 242s-250s.

Waszink, J.H., and G.J.F.M. van den Heuvel, 1982. Welding J., 61, pp 269s-282s.

Waszink, J.H., and L.H.J. Graat, 1983. Welding J., 62, pp 108s-116s.

Waszink, J.H., and M.J. Piena, 1985. Welding J., 64, pp. 97s-102s.

Waszink, J.H., and M.J. Piena, 1986. Welding J., 65, pp 289s-298s.

Woods, R.A., 1980. Welding J., 59, pp 59s-66s.